Evolution of the Thermohaline Structure of One Agulhas Ring Reconstructed from Satellite Altimetry and Argo Floats

R. Laxenaire, S. Speich, A. Stegner

JGR Oceans

RESEARCH ARTICLE
10.1029/2018JC014426

Evolution of the Thermohaline Structure of One Agulhas Ring Reconstructed from Satellite Altimetry and Argo Floats

R. Laxenaire[1,2], **S. Speich**[1], **and A. Stegner**[1]

[1]Laboratoire de Meteorologie Dynamique, LMD-IPSL, UMR 8539, Ecole Polytechnique, ENS, CNRS, Paris, France, [2]Center for Ocean-Atmospheric Prediction Studies, Florida State University, Tallahassee, FL, USA

Key Points:
- Lagrangian reconstruction of an Agulhas Ring sampled by an Argo float for more than 1.5 years
- In situ evidence of the subduction of an Agulhas Ring
- The reconstructed Agulhas Ring is characterized by two mode water cores

Correspondence to:
R. Laxenaire
rlaxenaire@fsu.edu

Citation:
Laxenaire, R., Speich, S., & Alexandre S. (2019). Evolution of the thermohaline structure of one Agulhas Ring reconstructed from satellite altimetry and Argo floats. *Journal of Geophysical Research: Oceans*, *124*, 8969–9003. https://doi.org/10.1029/2019JC015210

Received 9 APR 2019
Accepted 27 OCT 2019
Accepted article online 6 NOV 2019
Published online 13 DEC 2019

Abstract The transfer of Indian Ocean thermocline and intermediate waters into the South Atlantic via the Agulhas leakage is generally believed to be primarily accomplished through mesoscale eddy processes, essentially anticyclones known as Agulhas Rings. Here we take advantage of a recent eddy tracking algorithm and Argo float profiles to study the evolution and the thermohaline structure of one of these eddies over the course of 1.5 years (May 2013–November 2014). We found that during this period the ring evolved according to two different phases: During the first one, taking place in winter, the mixing layer in the eddy deepened significantly. During the second phase, the eddy subsided below the upper warmer layer of the South Atlantic subtropical gyre while propagating west. The separation of this eddy from the sea surface could explain the decrease in its surface signature in satellite altimetry maps, suggesting that such changes are not due to eddy dissipation processes. It is a very large eddy (7.1×10^{13} m^3 in volume), extending, after subduction, from a depth of 200–1,200 m and characterized by two mode water cores. The two mode water cores represent the largest eddy heat and salt anomalies when compared with the surrounding. In terms of its impact over 1 year, the north-westward propagation of this long-lived anticyclone induces a transport of 2.2 Sv of water, 0.008 PW of heat, and 2.2×10^5 kg s^{-1} of salt. These results confirm that Agulhas Rings play a very important role in the Indo-Atlantic interocean exchange of heat and salt.

Plain Language Summary The transfer of the Indian Ocean waters to the South Atlantic Ocean is generally believed to be primarily accomplished through anticyclonic eddies known as Agulhas Rings. There have been various studies investigating these eddies from sparse in situ and satellite observations. Here we take the advantage of the complementary information provided by eddies detected from satellite maps and free-drifting profiling floats measuring the upper 2,000 m of the ocean, to reconstruct the internal structure of one of them. This reconstruction shows that this Agulhas Ring quits the surface layer and slowly sinks into the subsurface as it drifts westward into the Atlantic Ocean. The ring is a very large eddy extending down to 1,200 m of depth and characterized by two cores showing temperature anomalies up to 4 °C when compared with the surrounding South Atlantic waters. These results confirm that Agulhas Rings play a very important role in the Indo-Atlantic interocean exchange of heat and salt.

1. Introduction

Mesoscale eddies are ubiquitous in the World Ocean (Chelton et al., 2011, 2007). Their energy generally exceeds that of the mean flow by an order of magnitude or more (Stammer, 1997; Wunsch, 1999) and they are thought to have a major impact on the spreading of hydrological properties by advecting them for considerable distances and over long periods. In particular, their influence is seen as key in the transfer of heat, salt, mass, and biogeochemical properties across the World Ocean (McWilliams, 1985).

Over the last 25 years, satellite altimetry has provided a regular, global, high-resolution monitoring of sea level and ocean circulation variations (Morrow & Le Traon, 2012). These data constitute a precious time series with regular spatial sampling capable of recovering around 60% of the variability in the 65 to 300 km mesoscale band (Pujol et al., 2016). For this reason, they allow us to quantitatively investigate the upper-ocean dynamics, and they have been shown to be particularly well suited to the study of mesoscale eddies (e.g., Chelton et al., 2011).

Since the early period of satellite altimetry, because of the large extent and intense altimetry signal of Agulhas Rings, various studies have focused on these Rings and their spatio-temporal evolution (e.g., Beron-Vera

et al., 2013; Byrne et al., 1995; Dencausse et al., 2010; Froyland et al., 2015; Gründlingh 1995; Guerra et al., 2018; Nencioli et al., 2018; Schouten et al., 2000; Wang et al., 2015, 2016). Agulhas Rings are mesoscale anticyclones spawned south of Africa by the South Indian western boundary current, the Agulhas, at its Retroflection. They are large (100 to 400 km diameter) rings of Agulhas Water that enter the Cape Basin southwest of Africa, before moving westward across the South Atlantic Ocean (e.g., Biastoch et al., 2009; Byrne et al., 1995; Guerra et al., 2018; Laxenaire et al., 2018; Schouten et al., 2000). The evolution and fate of Agulhas Rings are important aspects, since these rings are thought to account for an significant percentage of Indian water leakage into the Atlantic (e.g., Gordon & Haxby, 1990; Goni et al., 1997; A. Doglioli et al., 2006). This leakage impacts the Atlantic meridional overturning circulation (AMOC) and the related meridional transport of heat, freshwater, and biogeochemical properties, by influencing its strength (van Sebille & van Leeuwen, 2007; Weijer et al., 1999, 2002), stability (Weijer et al., 2001), and variability (Biastoch et al., 2008; Biastoch & Böning, 2013). Satellite data give access to the evolution of the surface properties of these eddies (e.g., Byrne et al., 1995; Froyland et al., 2015; Guerra et al., 2018; Souza et al., 2014; Laxenaire et al., 2018; Lehahn et al., 2011; Schouten et al., 2000). In particular, the above-mentioned studies show that the surface signature of Agulhas Rings decreases dramatically west of the Agulhas Retroflection and across the southern Cape Basin and continues to decrease gradually across the South Atlantic Ocean (e.g., Froyland et al., 2015; Guerra et al., 2018; Laxenaire et al., 2018). However, the majority of the previous studies based on satellite altimetry and with the aim of recovering the complete trajectories of one or more Agulhas Rings were not able to track all of them back from their area of Retroflection documenting their first detection in the vicinity of the Cape Basin (e.g., Byrne et al., 1995; Lehahn et al., 2011; Souza et al., 2014; Guerra et al., 2018).

This is most likely due to the non-consideration by previous studies of the complex nature of Agulhas Ring trajectories that undergo many eddy splitting and merging events (Schouten et al., 2000; Dencausse et al., 2010; Kersalé et al., 2018; Laxenaire et al., 2018). For example, studying Agulhas Rings in the Cape Basin, Dencausse et al. (2010) showed that the number of these eddies entering the Basin is multiplied by a factor of two when considering eddy splittings. Moreover, when focusing on the evolution and dissipation of three specific Agulhas Rings, Nencioli et al. (2018) observed a merging of two of them in the vicinity of the South Atlantic Ocean. Consequently, these interactions, impacting the pattern of the eddy evolution and dissipation, are important if we are to understand the mechanisms of ocean circulation and how Agulhas Rings influence the Earth's climate. Indeed, in the published literature it has been documented how Agulhas Ring surface properties change and how their disappearance from satellite altimetry maps is often associated with eddy dissipation processes, albeit direct observations of the latter are lacking. On the other hand, when these eddies are tracked over longer distances and for longer periods, and explicitly taking into account eddy mergings and splittings (Laxenaire et al., 2018), intense variations of their surface properties appear to be intimately correlated with such events.

Another limitation of satellite observations is that they do not provide information about the eddy vertical structure and how this evolves en route. Agulhas Rings have only been sampled occasionally by in situ observations from ships in the Cape Basin (e.g., Arhan et al., 1999, 2011; Casanova-Masjoan et al., 2017; Duncombe Rae et al., 1992, 1996; Garzoli et al., 1999; Gladyshev et al., 2008; Gordon et al., 1987; McDonagh et al., 1999; Schmid et al., 2003; van Ballegooyen et al., 1994), in the Southeast Atlantic (McCartney & Woodgate-Jones, 1991; Arhan et al., 1999), or from Argo profiling floats (Souza et al., 2011; Nencioli et al., 2018). However, with the exception of the observations reported in Nencioli et al. (2018), Souza et al. (2011), and Arhan et al. (1999), Agulhas Rings have not been sampled by in situ observations farther west of the Southeast Atlantic nor has it been possible to evaluate accurately their internal evolution from the Agulhas Retroflection onward. Concerning this last point, Schmid et al. (2003) and Nencioli et al. (2018) reported on the en-route evolution of Agulhas Rings. Schmid et al. (2003) discussed an Agulhas Ring sampled twice, at 6-month intervals, in the southern Cape Basin which showed an intense change of the upper-layer eddy properties (essentially in terms of temperature and density, very likely due to strong seasonal air-sea interactions) and a freshening of intermediate waters. Nencioli et al. (2018) also considered the intense variation of properties in the upper 200 m of an Agulhas Ring crossing the South Atlantic and discussed the modifications in the internal structure of this eddy. Moreover, the internal structure of this eddy was characterized by a subsurface core of homogeneous water that the authors identified as Mode Waters (MWs), in line with previous observations of subsurface intensified structures discussed by Arhan et al. (1999).

MWs are thick layers of homogeneous subsurface waters whose existence is thought to depend, as a precondition, on the formation of deep mixed layers (e.g., Hanawa & Talley, 2001). MWs have been identified

in every ocean basin, always on the warm side of a current or front (e.g., McCartney, 1977; McCartney, 1982; Hanawa & Talley, 2001). They are generally distributed below the surface far beyond their formation areas. Among these are western subtropical mode waters (WSTMW) usually associated with subtropical gyres and subantarctic mode waters (SAMW) associated with the subpolar fronts on the poleward boundaries of the southern hemisphere subtropical gyres (e.g., McCartney, 1977; Hanawa & Talley, 2001). MWs are correlated with large surface heat loss from the ocean and their low potential vorticity arises as a result of convection (e.g., Hanawa & Talley, 2001). Various MWs in the South Atlantic are discussed in the literature. Of these, Provost et al. (1999) documented from repeated hydrographic cruises two types of MW: the South Atlantic Subtropical Mode Water (SASTMW) found in the western subtropical gyre and the South Atlantic Eastern Subtropical Mode Water (SAESTMW) observed at the eastern edge of the subtropical gyre. Sato and Polito (2014) introduced a new definition of SASTMW by analyzing Argo float data. Using a clustering method they found three different varieties of SASTMW that differed in their hydrological properties and geographical location. These do not correspond completely with Provost et al. (1999)'s SASTMWs definition as they are defined from many more vertical profiles and over a larger area of the South Atlantic. It should be noted here that, using the eddy database from Chelton et al. (2011), Sato and Polito (2014) checked whether SASTMWs were correlated with the presence of mesoscale eddies. They did not find a high correspondence. However, when these authors did observe a correspondence between SASTMW and eddies, they found that 75% of them were anticyclones.

Very recently, de Souza et al. (2018) described the origin of South Atlantic MWs by decomposing thermocline waters as a product of the mixing of different MW varieties. They identified, among others, a particular SASTMW that is located along the Agulhas Rings main route where they are an important contributor of thermocline water. In addition, de Souza et al. (2018) identified a westward deepening of SASTMW where this mixes with MWs originating from the Indian Ocean. They attributed such a deepening to a sinking of the core of Agulhas Rings during their crossing of the South Atlantic. This echoes Herbette et al. (2004), who numerically demonstrated that Agulhas Rings could subduct below a front. Taking into account these works we might ask whether Agulhas Rings might be an active process of MW formation as speculated by de Souza et al. (2018), and whether the variations of surface properties observed in the altimetry maps are linked with lateral mixing of waters between the eddy core and the environment, or result from a different process acting on the internal properties of eddies. Finally, by using in situ data, numerous authors (Arhan et al., 1999, 2011; Casanova-Masjoan et al., 2017; Duncombe Rae et al., 1992, 1996; Garzoli et al., 1999; Gladyshev et al., 2008; Gordon et al., 1987; McDonagh et al., 1999; McCartney & Woodgate-Jones, 1991; Schmid et al., 2003; van Ballegooyen et al., 1994) have provided various estimates of Agulhas Ring volume, heat, and salt transports. It would be interesting to examine how this series of observed Agulhas Rings compare with each other and whether any general information about Agulhas Rings distribution can be derived.

In order to provide an additional step forward in the assessment of Agulhas Ring dynamics and changes across the Atlantic, we discuss here the evolution of one of these eddies in the South Atlantic, sampled by a high number of vertical profiles over more than a year. By making sure that the Argo profiles we used were meaningful observations of the eddy core, we isolated a period of the eddy lifetime during which the eddy subducted below the upper-ocean layer and where thermohaline properties remained steady. During such a period of time, the eddy structure might be considered sufficiently stationary to permit a meaningful reconstruction. By undertaking a comprehensive comparison with Agulhas Ring properties discussed in the literature, we proved the robustness of our results and highlighted the role of specific MWs responsible for important heat and salt content anomalies with regard to the surrounding waters.

The paper is organized as follows. In section 2, the data we have used are described, and the methods we have developed are presented. In section 3, the evolution of the surface and vertical eddy characteristics derived from satellite altimetry and Argo profiles is presented, as well as the reconstruction of the Agulhas Ring's mean internal structure in the South Atlantic. Section 4 discusses the results we obtained in the context of previous studies and assessments. A summary of the study and our conclusions about the results are provided in section 5.

2. Data and Methods

2.1. The South Atlantic Eddy Atlas

We selected Agulhas Rings from the South Atlantic eddies we identified and tracked them in time with the Tracked Ocean Eddies (TOEddies) automatic detection algorithm (Laxenaire et al., 2018) applied over more than 24 years (01/1993 to 05/2017) of the "all-sat-merged" series (Duacs/AVISO+, 2015) of delayed time

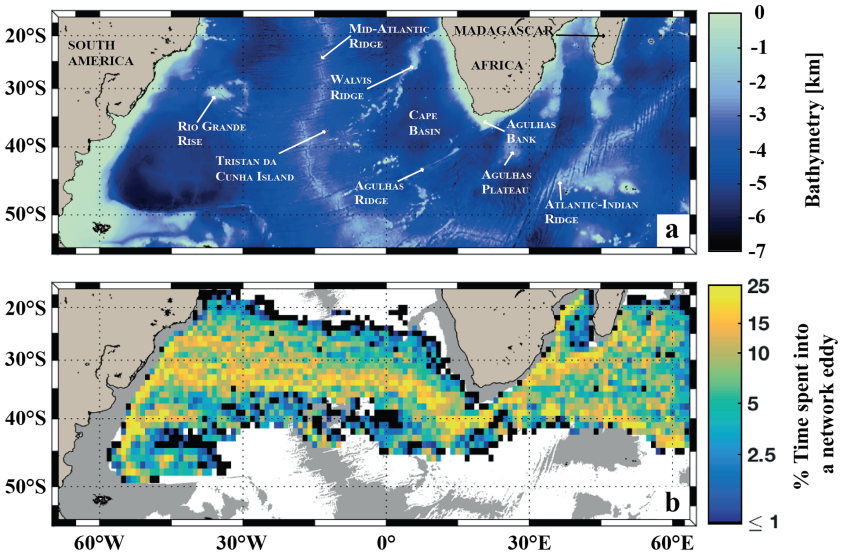

Figure 1. The study domain presented in terms of (a) the local bathymetry from the ETOPO2 data set (Smith & Sandwell, 1997) and (b) the percentage of time each 2° ×2° grid cell is occupied by the core of an eddy occurrence as part of the Agulhas Ring Eddy Network (Laxenaire et al., 2018). Figure modified from Laxenaire et al. (2018).

daily satellite altimetry maps gridded at 1 /4° in the South Atlantic and Southeast Indian oceans [70°W-65°E; 55°S-15°S] (Laxenaire et al., 2018) (see Figure 1a.). The TOEddies method is based on the algorithm proposed and developed by Chaigneau et al. (2008), Chaigneau et al. (2009), and Pegliasco et al. (2015). The eddy detection algorithm is a two-step process: It identifies the occurrences of eddies before deriving their trajectories.

The key assumption of eddy detection by the TOEddies algorithm is that mesoscale eddies satisfy the geostrophic balance. Therefore, the instantaneous eddy streamlines should coincide with the closed isolines of the daily absolute dynamic topography (ADT) maps. First, TOEddies identifies the local extrema (maxima and minima) of ADT by comparing each ADT grid point to its eight neighbors as possible eddy centers in the same way that other methods defined extrema from sea level anomaly (SLA) maps (e.g., Chelton et al., 2011; Faghmous et al., 2015). Next, it looks for the outermost closed ADT contour around each extremum. The module of the ADT difference between the extremum and this contour defines the amplitude of the detected eddy, which is considered a proxy of the eddy (surface) intensity. To filter out weak extrema we require that the extremum amplitude is greater than a threshold of 1×10^{-3} m. This value, which is small in comparison to the precision of satellite altimetry maps, was obtained by Laxenaire et al. (2018) to improve the coherence between the TOEddies Atlas and eddies identified from surface drifting buoys by Lumpkin (2016). The requirement to take into account eddies associated with amplitudes smaller than 1×10^{-2} m was demonstrated by Faghmous et al. (2015).

In addition to the outer closed ADT contour, TOEddies also identifies the contour where the azimuthal velocity of the eddy is at its maximum. This contour, associated with the gradient of the ADT, is expected to be less dependent on the hydrological structures out of the eddies and easier to compare with in situ data. TOEddies uses for this purpose the geostrophic velocity derived from ADT maps and computes along each closed contour the mean azimuthal velocity $< V >$. The contour, corresponding to $V_{max} = max(< V >)$, is called the characteristic eddy contour. The area of the eddy within this contour defines what we designate as the eddy core. The mean radius, R_{Vmax}, of this eddy-core area, A_{Vmax}, is derived according to the following equation:

$$R_{Vmax} = \sqrt{\frac{A_{Vmax}}{\pi}}. \quad (1)$$

We call this the speed radius because it is associated with V_{max}. In the same way, TOEddies defines the maximum radial extent R_{out} associated with the outer closed contour of the eddy. This limit is important as the eddy core defined by R_{Vmax} cannot be used alone to define either the area of influence of the eddy or the surface limiting the portion of the eddy where waters are trapped within the structure. This can

be better understood by considering the ratio between the eddy azimuthal and drift speeds. This ratio is a nonlinear parameter delimiting the area of water trapped in a coherent structure (Chelton et al., 2011; Flierl, 1981). For example, Agulhas Rings are characterized by a drifting speed of about 5–8 $\times 10^{-2}$ m s^{-1} (e.g., Casanova-Masjoan et al., 2017; Guerra et al., 2018; Nencioli et al., 2018) whereas V_{max} is of the order of several 10^{-1} m s^{-1} (e.g., Casanova-Masjoan et al., 2017). This suggests that water outside of the limit of R_{Vmax} can be trapped within these eddies. This is confirmed by Souza et al. (2011) who identified, in the South Atlantic, a horizontal extension of the eddy-trapped waters region larger than 150 km, whereas the typical R_{Vmax} of Agulhas Rings is, in this area, 60–80 km (Guerra et al., 2018; Nencioli et al., 2018; Laxenaire et al., 2018).

At this stage of the TOEddies algorithm sequences, the eddy center corresponds to the local extremum of ADT, which corresponds to a defined AVISO map grid point that might not coincide with the position of the eddy center. To avoid such a constraint, TOEddies computes the centroid of the eddy-core area to determine the geometrical center of the eddy. Finally, the TOEddies algorithm computes the vortex Rossby number (Ro) that we use to quantify the (surface) eddy intensity (e.g., Chelton et al., 2011; Mkhinini et al., 2014; Le Vu et al., 2018; Laxenaire et al., 2018). Ro is given by the following equation:

$$Ro = \frac{V_{max}}{f \times R_{Vmax}}, \tag{2}$$

where f is the Coriolis parameter.

In order to follow the position of each detected structure, TOEddies uses an algorithm based on the overlapping of eddy contours at consecutive time steps (Pegliasco et al., 2015; Laxenaire et al., 2018). Using the daily AVISO fields, the method relies on the fact that mesoscale eddies move slowly (displacements of less than 10 km.day^{-1}; e.g., Chelton et al., 2011; Garzoli et al., 1999; Laxenaire et al., 2018) relative to their typical radii which span the range 20–200 km (Carton, 2001). Consequently, the areas occupied by an eddy for two consecutive days overlap, and this can be used to track eddies (Pegliasco et al., 2015). Laxenaire et al. (2018) determined that the optimal percentage of the eddy area overlapping between two consecutive days was equal to or larger than 50% of the smallest area among the two eddies. This parameter reduces the number of spurious identifications (Laxenaire et al., 2018). If no eddy satisfies the condition of area overlapping for consecutive time steps, the research is extended for up to 5 consecutive days (i.e., half of the 10 days used by Le Vu et al., 2018), leaving the overlapping parameter unchanged.

The main advantage of the TOEddies tracking method is that it also allows for taking into account the merging of eddies, that is, when two or more eddies coalesce together to form one eddy, as well as the splitting of one eddy into two or more smaller eddies. Laxenaire et al. (2018) and Le Vu et al. (2018) have shown that merging and splitting events strongly impact the reconstruction of eddy trajectories and lifetimes. When these events occur, the segments of trajectories are reconstructed by associating pairwise eddies. In the case of a splitting, a cost function (CF), modified from Pegliasco et al. (2015) and Le Vu et al. (2018) and presented in equation 3, is applied to the eddy parent and the two or more eddy descendants. The CF compares changes (Δ) in the position of the eddy center (Center), Rossby number (Ro), and radius of maximum speed (R_{Vmax}) of the eddies where $\overline{\Delta\alpha}$ and $\sigma_{\Delta\alpha}$ denote, respectively, the mean and the standard deviation of the differences of a variable computed from all the association of eddies either during a splitting or a merging event. The two trajectory segments that minimize CF are identified as the main trajectories whereas the remaining segments are identified as the product of the splitting and referred to higher order trajectories (Laxenaire et al., 2018). Similarly, main trajectories are identified in the case of a merging.

$$CF = \sqrt{\left(\frac{\Delta\text{Center} - \overline{\Delta\text{Center}}}{\sigma_{\Delta\text{Center}}}\right)^2 + \left(\frac{\Delta\text{Ro} - \overline{\Delta\text{Ro}}}{\sigma_{\Delta\text{Ro}}}\right)^2 + \left(\frac{\Delta R_{Vmax} - \overline{\Delta R_{Vmax}}}{\sigma_{\Delta R_{Vmax}}}\right)^2}. \tag{3}$$

In this study, we consider trajectories whose lifetime is equal to or longer than 1 month (i.e., 4 weeks) to reduce the size of the database. This selection is reasonable in the case of Agulhas Rings that have, on average, a lifespan of a few months to several years (e.g., Byrne et al., 1995).

2.2. Sea Surface Temperature

It was shown by Lehahn et al. (2011) and Souza et al. (2014) that Agulhas Rings crossing the Atlantic Ocean can be associated with specific surface properties. In this framework, we will use sea surface temperature (SST) data to characterize the eddies. For this purpose we retrieved the level 4 ODYSSEA SST daily

database (Dash et al., 2012; Martin et al., 2012) produced by the Group for High Resolution Sea Surface Temperature (GHRSST) at Ifremer/CERSAT (France). These daily cloud-free SST maps are obtained using an optimal interpolation on a global gridded at 1/10° over the full globe merging both microwave and infrared satellite SST.

2.3. Argo Profiles Data and Eddy Colocation

While altimeter measurements are representative of the vertically integrated effect of variations in temperature and salinity over the whole water column, ADT maps do not allow for directly obtaining the vertical hydrological structure of the water column. To gain insights on this, we colocated the Agulhas Rings identified by TOEddies with in situ observations obtained from vertical profiles of the Argo floats international program which started in 2000. Argo floats provide a large number of CTD (conductivity, temperature, and depth) vertical profiles (i.e., more than 1.5 million profiles) over the upper 2,000 m of the global ocean. These data are collected and made freely available by the International Argo Program as part of the Global Ocean Observing System and the national programs that contribute to it (doi: https://doi.org/10.17882/42182). Argo Data Centers provide delayed mode data for each vertical profile. These data are validated and calibrated by the data assembly centers (e.g., Cabanes et al., 2016; Owens & Wong, 2009) against the most up-to-date global climatology (computed with both full depth CTD from oceanographic research cruises and validated Argo floats) to estimate errors for each Argo profile. However, because mesoscale eddies can have the ability to advect water from remote regions, the water trapped in the eddy core might have a distinct hydrological signature with respect to the surrounding climatological environment. Indeed, Argo profiles close to an eddy center significantly differ from the environment (e.g., Chaigneau et al., 2011; Pegliasco et al., 2015). Therefore, in this study, we use the Argo data downloaded from the Coriolis Global Data Center (Coriolis GDAC; http://www.coriolis.eu.org) that are not in the delayed mode but with control quality flags equal to 1 and 2, which refer to "good observation" and "probably good observation".

Because data from Argo profiles are usually not recorded at constant pressure levels, we have built a homogeneous data set by interpolating the temperature and salinity on a constant vertical grid of 10 m step. Furthermore, we applied an additional selection of Argo profiles, following Chaigneau et al. (2011) and Pegliasco et al. (2015), to ensure the consistency of the interpolation. First, we kept a profile if it contained at least one measure between the surface and 20 m and one below 1,500 m. Then, we required that the vertical distance between two consecutive measurements not exceed a given threshold, depending on the depth interval. These limits are 25, 50, 75, 100, and 200 m between, respectively, the depth intervals 0–100, 100–300, 300–500, 500–1,000, and below 1,000 m. This procedure removes about 40% of the profiles. Finally, we used the Gibbs SeaWater (GSW) Oceanographic Toolbox of the Thermodynamic Equation of SeaWater TEOS-10 (McDougall & Barker, 2011) to compute the recommended hydrological variables, which are the conservative temperature (Θ), the absolute salinity (SA), and the potential density anomalies referenced to the ocean surface (σ_0).

When based on the Argo system, Lebedev et al. (2007) showed that every Argo float moves, on average, about 4 km in 8 hr at the surface while sending eight messages to the satellite. Consequently, a typical lag of 1 hr can occur between the time the Argo float reaches the surface and the time its position is recorded by an Argos satellite. This time lag may induce an error in the position of the hydrological profile of the order of 500 m, which is small compared to the typical radii of mesoscale eddies (Carton, 2001) as well as the resolution of satellite altimetry from which eddy centers and shapes are identified. It is therefore possible to determine if a given hydrographic profile is located inside a detected eddy (e.g., Chaigneau et al., 2011; Pegliasco et al., 2015). The outer limit R_{out} is used for this determination as the trapped water in the eddy is not expected to be limited to the R_{Vmax} contour as previously discussed.

The colocation of Argo profiles and the TOEddies eddies results in the separation of such profiles into three groups: those sampling a cyclonic eddy, those sampling an anticyclonic eddy, and those falling outside of either type. We define the latter as profiles sampling the environment within which eddies propagate. In order to quantify the hydrological anomalies associated with each eddy, we computed a climatological profile characteristic of the environment outside that eddy which is then subtracted from the vertical profile sampling the core of the eddy. The climatological profile is the average of all the profiles measuring the environment outside the eddy. However, we require that their position falls within a rectangular box of of 2.5° ×2.5° centered on the eddy and whose dates are within a maximum temporal range of 30 calendar days (i.e., independently of the year) from the date of the Argo profile sampling the eddy. We tested both the spatial and time thresholds in order to find the best fit while keeping enough profiles and being sufficiently restrictive by not considering different hydrological regions or seasons to characterize the environment. Finally,

we estimated the distance between each profile and the geometrical center of the eddy. This distance from the center will be referred as *Dc* in the rest of this article.

3. Results

We followed Laxenaire et al. (2018) in creating the eddy network associated with the Agulhas Ring identified in the South Atlantic Eddy Atlas. In that context, Agulhas Rings are defined as the anticyclonic eddies which are initially detected in the Southeast Indian Ocean and then enter and propagate into the South Atlantic. The limit used to separate these two basins is an imaginary line connecting specific topographic structures, such as the Agulhas Ridge that defines the southeastern limit of the Cape Basin (Figure 1a). As shown by Dencausse et al. (2010), Agulhas Rings generally experience numerous mergings or splittings during their lifetime. Hence, several segments and bifurcations of trajectories have to be associated to correctly depict the whole lifespan for these eddies. In what follows, we will make use of the concept of the Agulhas Ring Eddy Network (AREN) of trajectories introduced by Laxenaire et al. (2018). This includes all the trajectories undertaken by any eddy, parent or descendant, that has merged with or split from a particular eddy or group of eddies originating in the Indian Ocean and traveling across the Indo-Atlantic limit.

The total AREN, defined during the period 1 January 2000 to 31 December 2016 (Laxenaire et al., 2018), is composed of 730,481 eddy occurrences (i.e., eddies detected in daily maps) that cluster into 6,363 trajectories. The percentage of time that each ADT grid point is inside the characteristic eddy contour of an eddy occurrence that is part of the AREN is presented in Figure 1b. The total AREN was sampled by 7,419 Argo profiles of which 826 sample Agulhas Ring main trajectories (i.e., a trajectory of an Indian anticyclone that flows into the South Atlantic basin).

Argo float No. 5902281 was identified as the one that was trapped for the longest period by a single Agulhas Ring, providing 54 vertical profiles over the period from May 2012 to November 2013, during which it propagated from Cape Basin to the Mid-Atlantic Ridge (Figure A1). The long trapping of this Argo float suggests that Agulhas Rings found in this region might behave as coherent eddies, at least at 1,000 m, which is the parking depth of these floats. This was also confirmed by other examples of float trapping by such eddies described in the literature. In particular, Nencioli et al. (2018) identified a comparable long trapping of an Argo float by an Agulhas Ring in this area between February 2014 and August 2015.

The AREN associated with the selected Agulhas Ring is presented in Figure 2. The main trajectory, as defined by the cost function, is composed of Segments 2, 5, and 6. The network, composed of seven segments, is a general example representing the relatively complex history of Agulhas Rings. It includes the various eddies and related segments of trajectory that have merged with and split from this Agulhas Ring during the 4 years and 7 months of its lifespan (from January 2011 to July 2015). Only the segments that interact directly with the main trajectory that trapped the Argo float No. 5902281 are discussed below. It is important to emphasize that, as the TOEddies Atlas could contain some spurious eddy merging and splitting events, we manually validated the particular Agulhas Ring trajectory we analyze in this study by excluding eddies that initially merge with and then split from this trajectory during times shorter than 1 week. The various eddies associated with this Agulhas Ring trajectory were sampled in total by 112 profiles from 19 different Argo floats. The number of the profiling floats together with their complete trajectories is presented in Figure A1.

The specific Agulhas Ring trajectory network that we analyze in this study starts with the shedding at the Agulhas Retroflection of three independent Agulhas Rings. The first shedding, which occurred on 8 January 2011, results in an eddy moving south and entering the Cape Basin by crossing the Agulhas Ridge (dark blue, Segment 1 in Figure 2) and following the Southern Agulhas Rings Route defined by Dencausse et al. (2010). The second and third shedding occur, respectively, in August and November 2011. The second shedding gives rise to an eddy whose trajectory (mid-blue, Segment 2 in Figure 2) follows the Agulhas Rings Central Route (Dencausse et al., 2010), whereas the third one (light blue, Segment 3 in Figure 2) takes the Northern Agulhas Rings Route (Dencausse et al., 2010). These two trajectories merge together in the eastern part of the Cape Basin forming Segment 4 of the AREN (green, Figure 2). The latter merges with the Southern Route eddy (Segment 1) in the northwestern part of the Cape Basin close to the Walvis Ridge. It results in Segment 5 (yellow line) that interacts with some other Agulhas Rings and anticyclones along its route but without any consistent merging and splitting events for 56 months until it reaches the South American Margin. There, in March 2015, it splits into two eddies that move south along the American continental slope until they disappear from the satellite altimetry field in July 2015.

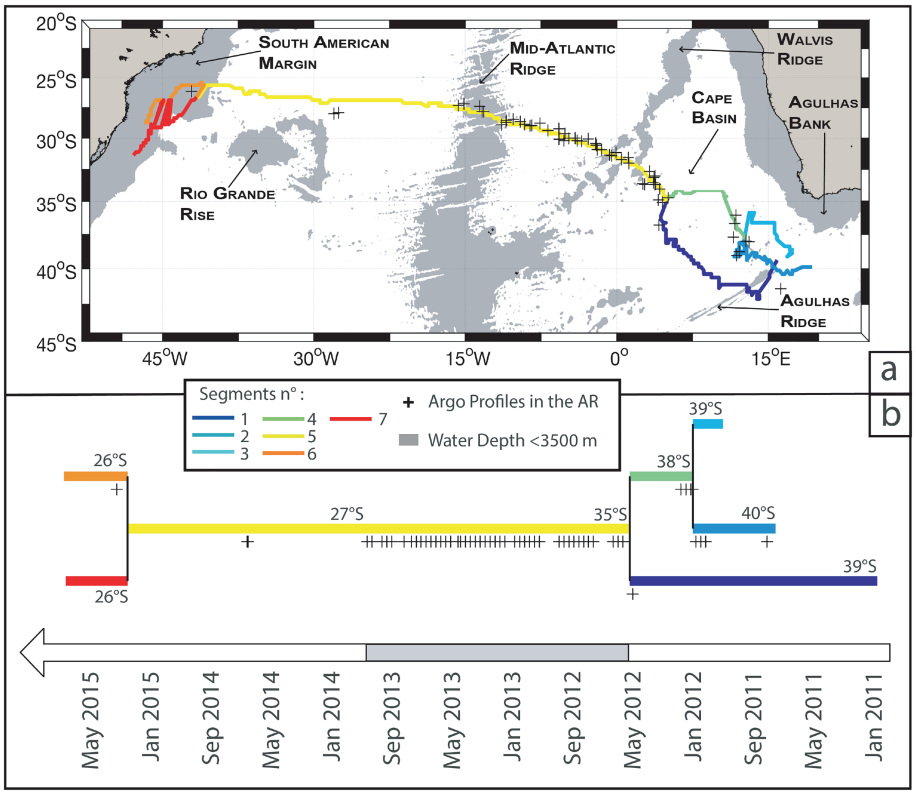

Figure 2. (a) Geographical distribution of the segments (in colors) that comprise the network of trajectories for the Agulhas Ring sampled for the longest period by an Argo profiling float. The positions of the Argo profiles sampling the eddy core of the whole set of eddies that comprised this particular network are represented by the black crosses; (b) a sketch displaying the various segments together with the eddy merging and splitting events and Argo profiles position as a function of time. The gray shading patches in (a) represent water depth shallower than 3,500 m in the ETOPO2 data set (Smith & Sandwell, 1997).

In this study, we focus on the period of time spanning May 2012 to November 2013, during which the Agulhas Ring did not merge or split while being relatively well sampled by multiple Argo floats (a profile sampled the structure at least every 10 days: See the black crosses in Figure 2). The data set combines 553 days of eddy detection from ADT maps and 71 Argo vertical profiles located within the core of the eddy and achieved by 14 different Argo floats. During this period, the anticyclone associated with Segment 5 leaves the Cape Basin, crossing the Walvis Ridge between October 2012 and January 2013; it then propagates in the eastern part of the South Atlantic before crossing the highest points of the Mid-Atlantic Ridge between August and October 2013 (see Figure B1).

3.1. Evolution of the Agulhas Ring surface dynamics

The temporal evolution of the surface signature of this Agulhas Ring (i.e., size and surface intensity) computed by TOEddies from ADT maps is presented in Figure 3. While R_{Vmax} of this eddy is rather constant during the entire period with a median value of 64 km associated with a small 8 km standard deviation (STD), R_{out} shows important variations (between 75 and 150 km and an STD of 23 km). To emphasize these differences, the evolution of the outer and characteristic contours (the latter is associated to V_{max}) is presented in Figure 4. Each contour is drawn in the translating frame of the Agulhas Ring where the position of the center of each figure corresponds to the center associated to the extrema of ADT. The contrast between the highly variable structure of the outer contour, which takes very complex shapes, and the characteristic contour, which remains coherent and keeps a relatively circular shape during the whole period of study, appears clearly. This difference might be due to the distortion of the edge of the eddy by the strain of neighbor eddies and the external flow field in general or to the small signal-to-noise ratio of the ADT outside of the eddy. In any case, we prefer to use the characteristic eddy contour and the corresponding speed radius R_{Vmax} to estimate the size of the structure, similarly to other algorithms (e.g., Nencioli et al., 2010; Duacs/AVISO+, 2017; Le Vu et al., 2018).

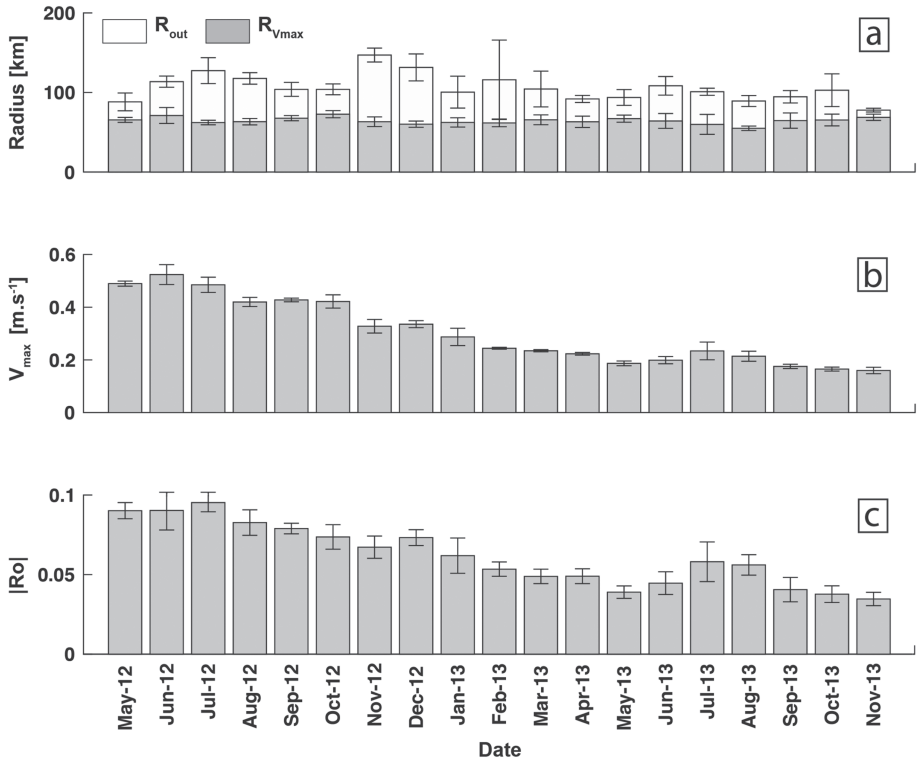

Figure 3. Temporal evolution of (a) the monthly averaged equivalent radius of the outer contour (R_{out}) and the eddy-core contour where the azimuthal velocity is maximum (R_{Vmax}); (b) the maximum azimuthal velocity (V_{max}); and (c) the absolute Rossby number of the core (|Ro|) as derived from the altimetry maps. The error bars correspond to the monthly STD of these parameters.

The evolution of the monthly mean V_{max} and Ro is shown in the lower panels of Figure 3. The maximum value of V_{max} is about 50×10^{-2} m s^{-1} in the end of the austral fall 2012. It then decreases gradually to smaller values, below 20×10^{-2} m s^{-1}, almost 1 year later. Figure 3 shows a similar decay for Ro. This is very likely due to the variation of V_{max} as the eddy size is constant and the meridional displacement is limited. One might argue that this decrease in surface intensity is related to the change of environment. However, the amplitude of the Agulhas Ring decreases from 0.4 to 0.1 m (not shown) during its journey while the variations of the MDT interpolated at the Agulhas Ring center do not exceed 0.1 m. A similar decay of surface intensity across the South Atlantic has already been documented by several authors (e.g., Byrne et al., 1995; Guerra et al., 2018; Laxenaire et al., 2018; Schouten et al., 2000). During the whole period, the Agulhas Ring absolute Ro remains small (below 0.1), which confirms that this eddy is balanced geostrophically and therefore we do not

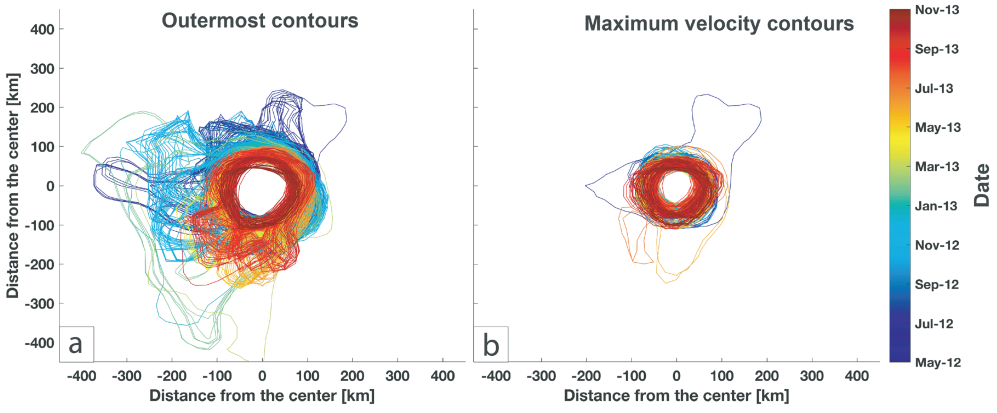

Figure 4. (a) Outer contours and (b) characteristic contours (associated with the maximum azimuthal speed) in the referential of the Agulhas Ring at times when an Argo float samples it.

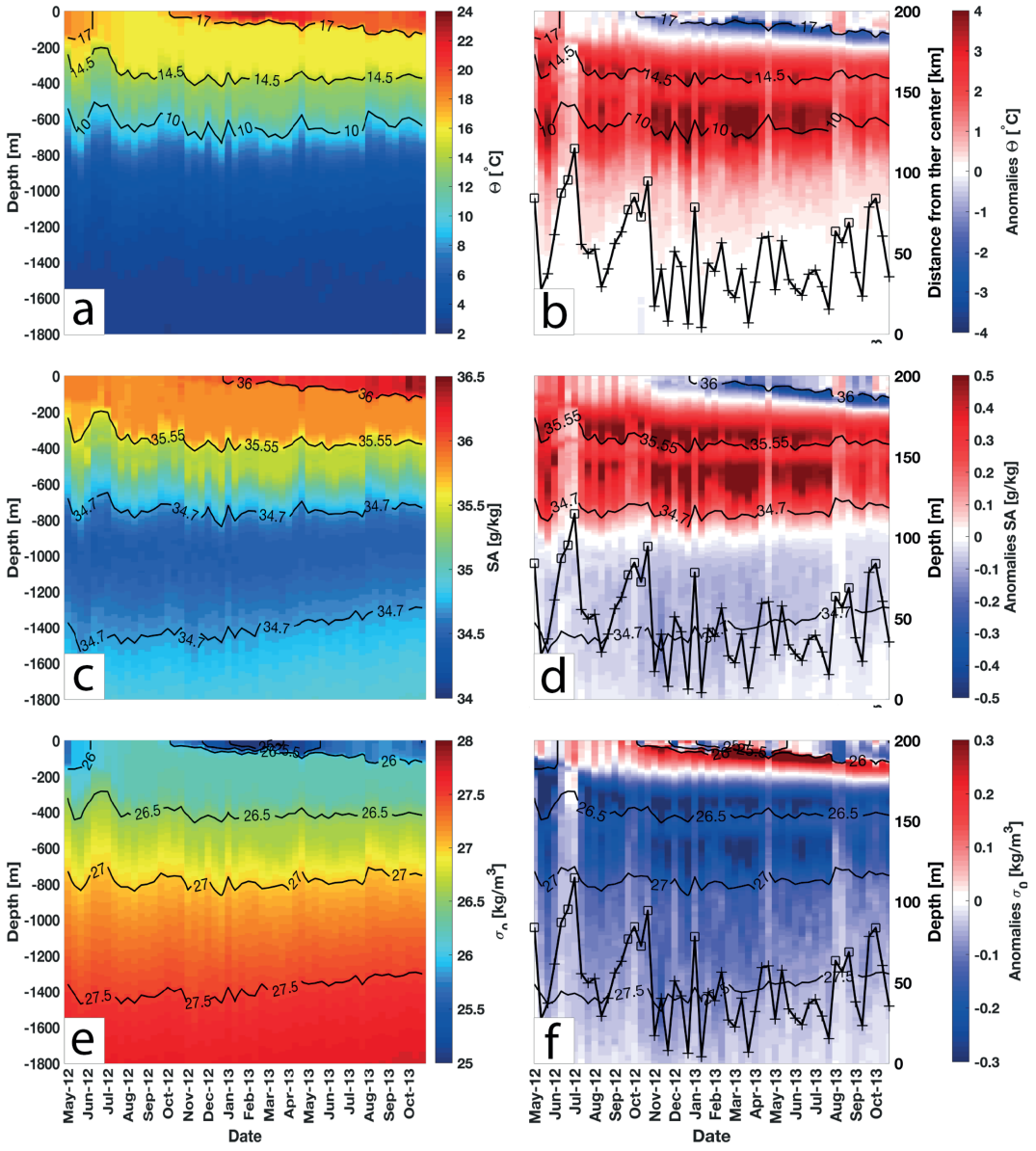

Figure 5. (a) Conservative temperature (Θ), (b) Θ anomaly, (c) absolute salinity (SA), (d) SA anomaly, (e) potential density (σ_0), and (f) σ_0 anomaly for the closest Argo profiles to the Agulhas Ring center for each 10 day interval as a function of time and depth. Black lines with markers in each right panel represent the distance of each profile from the eddy center (Dc) whose scale is presented on the *y*-axis on the right of panels (b), (d), and (f). The marker is a cross for profiles inside the characteristic contours; otherwise it is indicated as a square. Selected isotherm, isohaline, and isopycnal levels are added to the corresponding panels for both the full fields and the anomalies.

need to apply the cyclo-geostrophic correction as in Ioannou et al. (2017). A short period of intensification is visible in winter during July and August 2013 and a final decay of the surface signature is visible during the two last months of the period under study.

3.2. Evolution of the Internal Structure

In order to estimate the evolution of the conservative temperature (Θ), absolute salinity (SA), and potential density (σ_0) inside the Agulhas Ring, we first divided the time period into 10 day intervals. For each of these 10 day intervals we selected the Argo profiles closest to the eddy center. The selected vertical profiles are presented in the left panels (a), (c), and (e) of Figure 5 and the associated anomalies, computed as the difference between the vertical profiles sampling the eddy and the mean environmental profiles, are presented in the right panels (b), (d), and (f) of the same figure together with the distance (Dc) of the Argo profile from the eddy center.

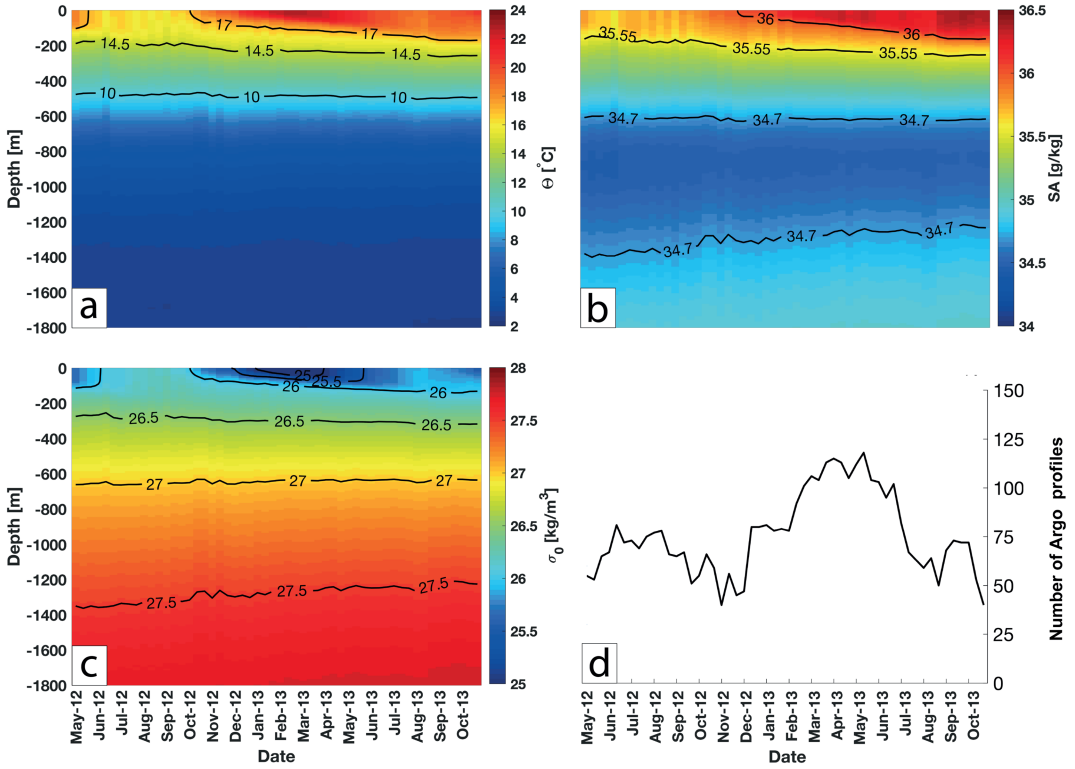

Figure 6. (a) Conservative temperature (Θ), (b) absolute salinity (SA), and (c) *potential density* (σ_0) for the environment climatological profiles we used to compute the Agulhas Ring vertical property anomalies in Figure 5; (d) number of averaged Argo profiles used to to compute the first 1,500 m of the environment climatology.

The climatologic profiles used to compute the anomalies as well as the number of profiles used to compute the first 1,500 m of each climatological profile at each time step are presented in Figure 6. For this study we selected only Argo profiles associated with a maximum depth of over 1,500 m. Indeed, the number of profiles sampling the upper layer of the water column is higher than those reaching depths of over 1,500 m. The minimum available profiles within the eddy core close to the surface is 40, but this decreases to 28 for profiles reaching a depth of 1,800 m (not shown). The maximum number of profiles is 118 for the upper 1,500 m of depth and 93 for profiles reaching 1,800 m (not shown). In the climatological profiles, the upper 200 m appear as the most variable. A surface layer of low density appears in October 2012 concomitant to the onset of the summer seasonal stratification as well as the drifting of the eddy into warmer waters. This limit, characterized by the isopycnal 26.2 kg m^{-3}, appears to continuously thicken during a period of more than a full year. The layers below this isopycnal show more steady characteristics during the full period, albeit a relatively small downlift of the isolines appears between a depth of 200 and 400 m and an uplift appears below 400 m. Very likely, this is due to the westward thinning of the Antarctic Intermediate Water (AAIW) layer marked by a minimum of salinity around 1,000 m as discussed by Rusciano et al. (2012).

Figure 5 presents the hydrological characteristics of the Agulhas Ring as provided by the Argo profiles sampling the eddy. It shows that important variations in the eddy properties occur in the upper 200 m. Here, a shallow and low-density layer (limited by the 26 kg m^{-3} isopycnal) is visible in May 2012 (during the end of the austral fall). This layer is eroded at the beginning of the austral winter (from June 2012) and reappears in October 2012 during the austral spring. This layer might be associated with the seasonal cycle, with the formation and erosion of a seasonal thermocline. However, similarly to the behavior shown by the climatological profiles (Figure 6), this layer continues to thicken from October 2012 to November 2013, not showing any further winter erosion. This suggests that the upper eddy layer not only evolves with the seasonal cycle but is also affected by the displacement of the eddy into a different hydrological region (the South Atlantic subtropical gyre) characterized by a shallow permanent stratification.

The Argo data also show a relatively high correlation between vertical properties and the distance (Dc) of the profile from the eddy center (see, for instance, the variations of Dc together with those of the isolines 10°C, 34.7 g kg^{-1}, and 27 kg m^{-3} in Figures 5a, 5d, and 5e). As expected for a warm and salty core anticyclone

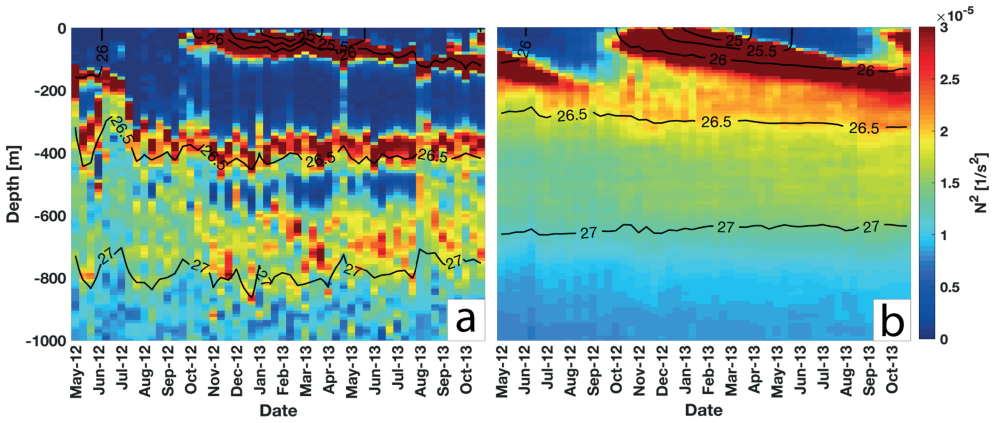

Figure 7. Time evolution of the Brunt Väisälä frequency squared (N^2) computed for the Argo float No. 5902281 profiles (a) within the Agulhas Ring, and (b) for the environment climatology. Isopycnal levels separated by a 0.5 kg^{-3} interval are added to the corresponding panels.

such as an Agulhas Ring, the isolines are deeper near the center of the structure than at its edges. The correlation among the eddy hydrological properties and Dc is particularly evident from the vertical Θ, SA, and σ_0 anomalies (Figures 5b, 5d, and 5f). Their amplitude variations are indeed intimately linked with Dc variability and this through the whole water column. In particular, Figures 5b, 5d, and 5f show clearly a strong reduction in the anomaly amplitude when Dc is larger than 65 km. This corresponds to the periods June–July 2012, October 2012, January 2013, and, later on, in August and October 2013.

The eddy property anomalies (Figures 5b, 5d, and 5f) show that the Agulhas Ring is warmer, saltier, and less dense than the environment. A marked positive anomaly in SA (>0.2 g kg^{-1}) and Θ (>1 °C) down to at least 800 m appears clearly for small Dc (Dc < 50 km). Moreover, theses anomalies exhibit a striking vertical pattern characterized, from November 2012 to August 2013, by two well-separated extrema roughly located at a depth of −350 and −650 m. Such a vertical structure strongly suggests the presence within the eddy of two cores of water masses very different from the environment. It should be noted here that σ_0 anomaly for the two distinct water mass cores is about −0.3 kg m^{-3}, a value six times higher than the STD of the environment σ_0 (0.05 kg m^{-3} [not shown]). It is worth noting that, after November 2012, negative anomalies of SA are found within the eddy below 1,000 m.

To better understand the vertical structure of the Agulhas Ring, we plotted the Brunt Väisälä frequency squared N^2 in the Argo profiles plotted in Figure 5 and the climatological environment in Figure 7. N^2 is computed from equation 4, where g is the gravitational acceleration and ρ_0 the density of reference set to 1,000 kg m^{-3}.

$$N^2 = \frac{-g}{\rho_0}\frac{\partial \rho}{\partial z}. \tag{4}$$

The environment profiles exhibit a seasonal cycle characterized by the development of a winter mixed layer (low values of N^2, below 1×10^{-5} s^{-2}) extending, on average, to a depth of 150 m in August–September (Figure 7b). On the other hand, the eddy core is characterized by a considerably deeper mixed layer which develops during the first 5 months of the time series and which reaches a depth of 350–400 m in August–September 2012. During this period, the eddy upper layers are connected to the sea surface and the atmosphere through this deep mixed layer. Later on, from October 2012 to March 2013, the summer restratification seems to isolate the eddy homogeneous cores from the surface and prevent any direct heat or momentum transfer between the eddy core and the atmosphere. Below this layer lies the uppermost of the two cores whose properties correspond to the previous winter mixed layer. Its properties are homogeneous over more than 200 m, suggesting that this core belongs to MWs.

Figures 5 and 7 suggest, therefore, that the main hydrological core of the eddy was connected with the sea surface and exposed to air-sea interactions during the first part of the time series and that it became a subsurface core, isolated by the presence of an upper stable and relatively thick (200 m) warm layer, while leaving the Cape Basin and entering the South Atlantic Ocean by crossing the Walvis Ridge (see Figure 2). This analysis is, of course, restricted by the limited availability of profiles close to the eddy center before July 2012. To corroborate our results, we undertook a satellite SST data analysis to try to assess the surface

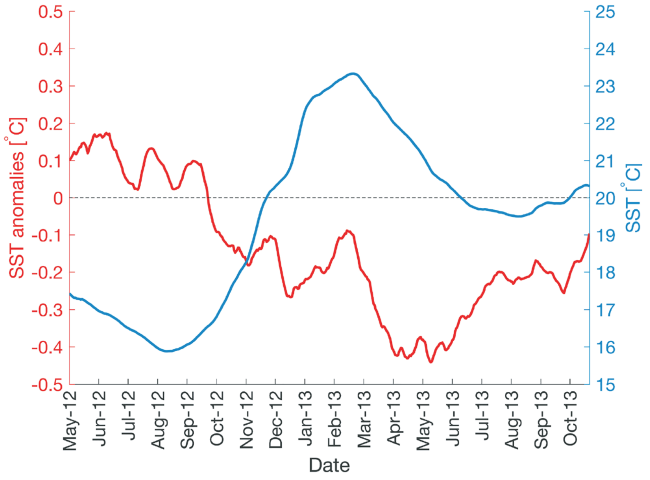

Figure 8. Sea surface temperature (blue) and associated anomalies (red) interpolated from the ODYSSEA SST data set (Dash et al., 2012; Martin et al., 2012) at the center of the Agulhas Ring. The anomalies are computed by subtracting the mean SST (computed as the average of the SST in the square box area of 300 km × 300 km centered on the eddy center) to the SST value in the center of the eddy. All the data were smoothed by a moving average associated with a monthly window.

signature of the eddy and to characterize its connection with the ocean surface layer in an independent way. This is in line with the works of both Assassi et al. (2016) and Schütte et al. (2016), who used surface SST anomalies to discriminate surface and subsurface intensified eddies. Indeed, anticyclonic eddies are associated with positive sea level anomalies. If they are surface eddies, they are expected to correspond to positive SST anomalies, whereas if they are subsurface eddies, they should be associated with negative SST anomalies as a consequence of the doming of the isotherm above their hydrological core.

For this purpose, we used the ODYSSEA SST dataset (Dash et al., 2012; Martin et al., 2012) that we have interpolated at the position of the eddy center during the period of interest (see Figure 8). For each date, we computed the average of the SST field for all the points in the square box area of 300 km × 300 km centered on the eddy center (i.e., 150 km corresponds to the maximum R_{out}). The anomalies are computed by subtracting this mean SST from the SST value at the center of the eddy. These anomalies are presented in Figure 8. It appears from this figure that they change sign between September and October 2012. This is in accordance with what we identified as the beginning of the isolation of the Agulhas Ring from the ocean surface, as previously discussed in the analysis of Figures 5 and 7. Such a change of sign can be due to the modification of the background environment while the eddy moves into subtropical waters. Yet the absolute SST (blue line in Figure 8) clearly shows a seasonal cycle as well as an interannual increase, indicating that variations also occurred within the eddy. It is not consistent with a fixed patch of constant temperature drifting into another environment. However, Souza et al. (2014) discussed the presence of negative SST anomalies in relation to Agulhas Rings still connected with the ocean surface. They explained this by a modification of the Ekman pumping due to the presence of the eddy and that it may induce dipole SST anomalies with the center of an Agulhas Ring associated to a negative SST anomaly, whereas a positive anomaly would correspond to the eddy boundaries.

To assess the geographical pattern of SST anomalies, we computed monthly SST anomaly maps in the moving frame of the Agulhas Ring. They are presented in Figure C1. These maps show that, in July 2012, the Agulhas Ring core is associated with positive SST anomaly values. These, however, are lower within the eddy's inner core than at its boundaries, which might confirm the conclusions of Souza et al. (2014). However, after October 2012, the date we identified as that corresponding to the isolation of the main hydrological core of the Agulhas Ring from the ocean surface, the SST dipole-like anomaly disappears and the Agulhas Ring becomes associated with a strong patch of negative SST anomalies, confirming the subsurface nature of the eddy following critera of Assassi et al. (2016) and Schütte et al. (2016). Positive anomalies still exist close to the eddy boundary but are localized at the eddy western side, a feature that can be explained by the stirring of the environment due to the anticlockwise rotation of the Agulhas Ring in the presence of a north-south gradient of temperature.

The results we obtained by analyzing two independent data sets (Argo vertical profiles and satellite SST) corroborate the finding that the main hydrological core of the Agulhas Ring, initially connected to the surface, subducted into the ocean interior while leaving the Cape Basin and penetrating into the South Atlantic subtropical gyre. We follow here Williams (2001)'s definition of subduction as the transfer of fluid from the mixed layer to the stratified thermocline (i.e., below the seasonal mixed layer). It is clear that the winter mixed layer developing between March 2013 and September 2013 stays separated from the shallower eddy core of homogeneous water. However, it is difficult to select the main process generating the observed subduction. Indeed, the observed behavior might result from a modification of the eddy upper-layer waters by ocean-atmosphere interactions Arhan et al. (2011) as well as by the lateral penetration of an eddy below the lighter upper water of the South Atlantic subtropical gyre.

In order to gain insight into this question, we evaluated (Figure D1) the differences in terms of T-S properties for Argo profiles sampling Segment 5 during the period November 2012 to November 2013 near the eddy center (Dc < 25 km, in red in Figure D1) and those close to the eddy boundaries (150 < Dc < 200 km, in blue in Figure D1). This analysis shows that the upper-layer eddy water masses are different to those of the environment. However, the eddy upper-water velocities still verify the eddy-coherent condition defined by

Flierl (1981) and used in many studies since then (e.g., Chelton et al., 2011): The minimum of V_{max} is larger than 0.2 m^{-1} (see Figure 3) while the drifting speed of the eddy does not exceed 0.1 m s^{-1}. This suggests that the observed subduction could result from the surface modification of the Agulhas Ring advected water. Using a very high-resolution numerical simulation in the Cape Basin, Capuano et al. (2018) showed that submesoscale instabilities (of different type) determine, in winter, the formation of deep mixing layers in Agulhas Rings and, in summer, induce an intense upper-layer restratification. As the Agulhas Ring moves westward exiting the Cape Basin, it enters a region of milder air-sea interactions that are not sufficiently strong to erode the upper-layer stratification. Such a process might explain the isolation of the Agulhas Ring subsurface core from the ocean surface.

Figure 7 reveals the presence, between October 2012 and August 2013, of a second, albeit thinner, homogeneous layer located deeper than the first one (between 500 and 600 m). It corresponds to the second thermohaline anomalies core that appears in the Argo vertical profiles sampling the Agulhas Ring (Figure 5). After August 2013, the Argo profiles sample the eddy farthest from the eddy center. This prevents any conclusion as to what makes this deeper core of MW disappear. Indeed, on August 2013, the eddy is located over the Mid-Atlantic Ridge(see Figure B1). We suggest that the interaction between the eddy and the topography caused an intense mixing at depth with neighboring waters. Or it might be that, because of the larger distance of the sampled profiles from the eddy center after August 2013, this core of MW that was probably small in its lateral extent was not sampled by the Argo floats.

To prevent the interference of the varying position of Argo floats while attempting to determine the eddy evolution in time, we select, in the following section, only those Argo profiles located within the eddy core (i.e., $Dc < R_{Vmax}$). The density anomalies associated with four profiles separated by 4 or 5 months between June 2012 and August 2013 are shown as solid lines in Figure 9a. All these profiles are located inside the eddy and close to its center (15 km < Dc < 30 km), albeit it is worth mentioning that accuracy in determining the eddy center from ADT maps is limited and this might induce significant errors in Dc estimates. For comparison, Figure 9a presents, in a dashed line, a vertical profile undertaken in January 2013 by an Argo float far from the eddy center (Dc = 151 km). From this figure, it appears clearly that this profile does not sample any of the eddy MW cores.

Figure 9b shows the depth of the two Agulhas Ring MW cores as a function of Dc computed by taking a large number of Argo profiles, all located near the eddy center (Dc < 40 km) and defined as the vertical maxima of thermohaline anomalies. The vertical location of the two thermohaline anomaly maxima varies weakly with time and with the distance of the Argo profile from the eddy center. We also computed the STD of the residual between each extremum and the linear regression obtained between Dc and the depth of the two anomaly peaks. We considered as outliers those profiles whose residuals are larger than the STD (Figure 9b). From this, it appears that two of the three profiles that sampled the eddy before it subsided below the surface in November 2012 differ significantly from the others. For the latter, the density anomaly of the core seems to keep roughly the same depth for several months.

3.3. Reconstruction of the Subsurface Structure of an Agulhas Ring

Figures 5 and 7 show that, from November 2012 to November 2013, the upper 150 m layer of water within the Agulhas Ring limits was characterized by a strong seasonal variability, whereas below it, the thermohaline properties underwent only small variations. We therefore assumed, as a first-order approximation, that the Agulhas Ring below a depth of 150–200 m was in a quasi-steady state and that the upper 150 m layer of water no longer belonged to the eddy main hydrological core.

Similarly to the assumptions of Souza et al. (2011) and Nencioli et al. (2018), we also hypothesized that the eddy had a quasi-circular symmetry. The amplitude of the subsurface anomaly will then depend only on the distance (Dc) between the Argo float position and the geometrical eddy center. As discussed previously, R_{Vmax} can be considered to be constant during at least the period November 2012 to November 2013 (with a median and mean radius of 63 km and an STD of 8 km). However, to test the validity of a quasi-circular eddy assumption, we estimated the ellipticity (ϵ) of the characteristic eddy contours derived from the daily ADT maps, from equation 5 where a is the semimajor and b the semiminor axis.

$$\epsilon = 1 - \frac{b}{a}. \tag{5}$$

The ellipticity remains small from November 2012 to November 2013, with a median value of 0.11, a mean of 0.12, and an STD of 0.07. We therefore restricted our analysis to this 12 month period to ensure the validity of the axisymmetry hypothesis for the eddy, which would otherwise not be valid for large ellipticity values.

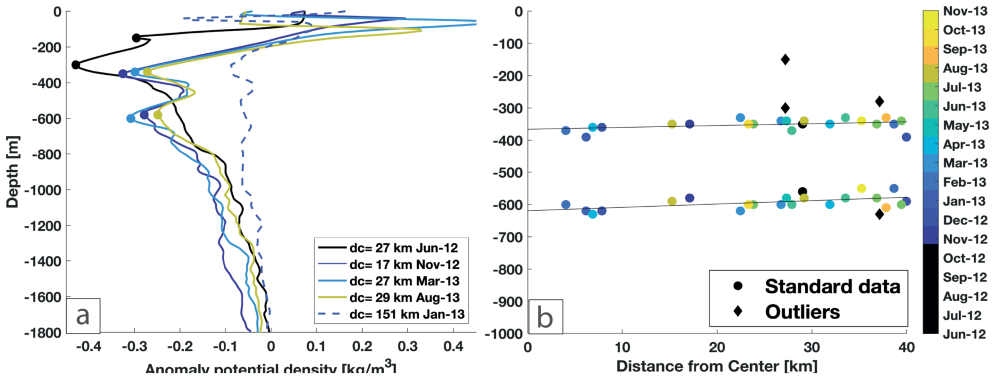

Figure 9. (a) Argo vertical profiles of density anomaly. Four lie close to the eddy center and show the two mode waters' thermohaline extrema (solid lines); one is located farther away (dashed lines) and does not display these two mode waters' related extrema. (b) Depth of the two mode water cores as a function of Dc for all the profiles lying at less than 40 km from the eddy center. An outlier is identified if both extrema in a profile are at a distance from the black lines greater than the STD associated with the determination of each extremum.

In order to reconstruct the Agulhas Ring axisymmetric structure, we used 71 Argo profiles that were located within a distance of 185 km (i.e., ~3 $\times R_{Vmax}$) from the geometrical eddy center (Figure 10) during the November 2012 to November 2013 period. The Argo float No. 5902281 sampled more than 54% of the profiles, whereas other floats surfaced sporadically inside the eddy. Overall, during the given 12 month period, the Agulhas Ring was sampled by 52 profiles within a distance of 100 km from the eddy center.

Different techniques have been used in the literature to attempt a reconstruction of the vertical structure of mesoscale eddies from sparse in situ observations. Most of them employed a composite eddy reconstruction approach (e.g., Amores et al., 2017; Schütte et al., 2016), while others tried to recover the structure of specific eddies. For example, Chaigneau et al. (2011) objectively mapped observations onto a 10 km grid assuming an isotropic Gaussian covariance decorrelation scale of 100 km, and Souza et al. (2011) fitted to a seventh order one-dimensional Lagrange polynomial. However, the Gaussian method smooths out horizontal gradients, whereas high-order polynomials often induce an overshooting of the hydrological variables at the outer edge of the reconstructed eddies. To avoid these drawbacks, we used a generic function tending towards zero outside the eddy.

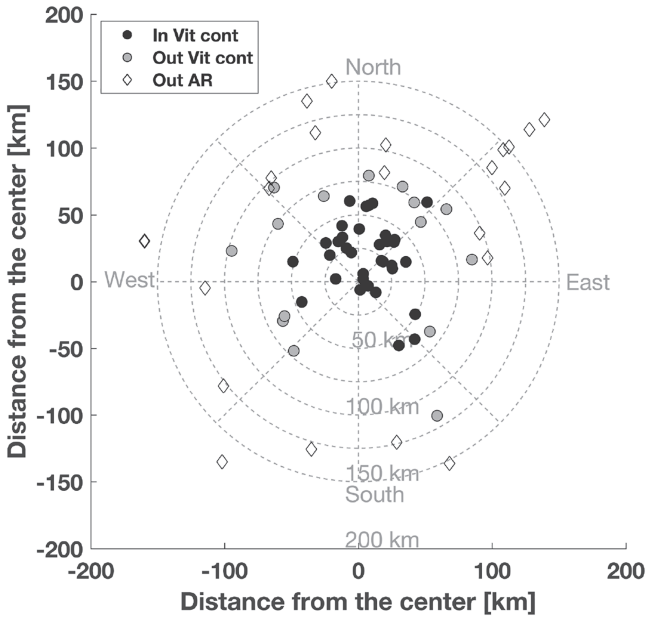

Figure 10. Position of the Argo profiles in the moving frame of the Agulhas Ring. The center of the frame corresponds to the centroid of the characteristic eddy contour delimited by R_{Vmax} and computed from ADT maps. The filled circles indicate Argo profiles inside the characteristic eddy contour, the gray circles those inside outer eddy edge, and the empty diamond those outside the Agulhas Ring and any other neighboring eddy and lying at a 160 km radius from the Agulhas Ring center.

The generic function we used to fit the (Θ and SA) anomalies we defined previously at each depth (see equation 6) is that of an α-Gaussian vortex (see, e.g., Carton, 2001; Le Vu et al., 2018; Zeitlin, 2018). The parity of this generic function ensures the axisymmetry of the reconstructed eddy and an exponential reduction in its anomalies far from the center. The $A_0(z)$ profile represents the maximal core anomaly inside the eddy. To suggest a first guess for $A_0(z)$, we use the mean of the three Argo profiles closest to the eddy center while the parameters α and $R_0(z)$ are set initially to 2 (i.e., a purely Gaussian shape as used by Nencioli et al., 2018) and R_{Vmax} = 63 km, respectively. Then, the three parameters (A_0, R_0, and α) associated with the generic function 6 are adjusted at each depth level, minimizing the residuals between the fitting of the equation and the observations using the Trust Region Reflective algorithm (Branch et al., 1999) with the function lsqcurvefit of the MATLAB Library. As we expect the anomalies to increase toward the center, we do not allow A_0 to be lower than the first guess which ensure to preserve the large scale gradient. Moreover, it is worth noting that the Trust Region Reflective algorithm can stop at local best fit; thus, several adjustments are run at each levels varying the initial guess of α and $R_0(z)$ to detect the global best

fit. Below 200 m, the values obtained for the various parameters by fitting the function 6 are between 1.9 and 2 with an STD between 0.05 and 0.15 depending of the variable. Similarly, mean R_0 is between 66 and 76 km with an STD ranging between 10 and 17 km.

$$Anom(r,z) = A_0(z)e^{-\frac{1}{\alpha}\left(\frac{r}{R_0(z)}\right)^{\alpha}}. \quad (6)$$

Finally, to obtain a first estimation of the thermohaline structure of the Agulhas Ring ($Anom(r,z)$), we added the average of all the profiles of the environment computed for each vertical level to the reconstructed anomalies.

Figure 11 shows the isolines of Θ, SA, and σ_0 for the reconstructed Agulhas Ring (defined with the acronym RecAR from here on), superimposed over the raw Argo profile data plotted as a function of Dc. A more detailed examination of the σ_0 reconstruction is shown in Figure E1. Both figures show, below the surface, a particularly good agreement between the isocontours of RecAR and the raw Argo data.

Figure 11 shows clearly two layers of homogeneous thermohaline properties. A first one is centered around a depth of 250 m, between the isolines 17–15 °C, 35.9–35.7 g kg^{-1}, and 26.1–26.3 kg m^{-3}. The maximal thickness of this layer is ~350 m at the eddy center. The second homogeneous layer is centered at a depth of 500 m, and it is characterized by the isoline intervals 13–11 °C, 35.5–35.3 g kg^{-1}, and 26.5–26.7 kg m^{-3}. One can observe that the depths of these cores do not correspond to those obtained from anomalies in Figure 9 but correspond well with the position of the N^2 cores at the end of the time series in Figure 7. Our impression is that the position of the maximum anomaly shows the depths of the bottom of each layer of MW just above the compensation that occurs below each MW. Consequently, the anomalies cannot be used to identify the center of a hydrological core.

In order to test the accuracy of the three-dimensional reconstruction, we computed the root mean square (RMSE) of the difference between the in situ measurements provided by every Argo profile and RecAR (Figure 11d). The values of RMSE vary between 0.01 and 0.05 kg m^{-3}, which is six times less than the maximum σ_0 anomalies. This gives us confidence in the eddy properties reconstruction.

The two local maxima at depths of 400 and 700 m in Figure 11 correspond to the region of strong variation of properties when moving from the eddy center outward along an constant line of depth. However, near the surface the errors are considerably larger. The RMSE value of 0.05 kg m^{-3} lies between a depth of 150 and 160 m whereas the largest RMSE value (0.2 kg m^{-3}) is found at 60 m. At these depths waters undergo a strong seasonal forcing, and therefore, we cannot consider that the thermohaline properties of the eddy remain constant here for the whole year. As discussed previously, the Agulhas Ring has subducted below the subtropical gyre upper 150 m of warm waters. Hence, we assume that the eddy upper limit is below this layer. We choose as such a limit for RecAR a specific isopycnal—the 26.2 kg m^{-3} isopycnal—which corresponds to the specific limit identified in Figure 5 as the separation between the part of the water column that evolves over time and the one which is steady below it, rather than a fixed depth. It is important to note here that the depth of this isopycnal varies between 150 m near the eddy center and 170 m away from it. In what follows, we will consider as RecAR the waters lying below the 26.2 kg m^{-3} isopycnal surface.

By using RecAR as the reference, we computed the error associated with the values of Dc obtained in colocating the Argo profiles with the eddy as detected by the TOEddies algorithm. A distance is computed between each observation on the σ_0 levels, between a depth of 200 and 1,000 m, from the Argo profiles and the corresponding value in the RecAR. This corresponds to the distance between each observation and the RecAR isoline taken at the same depth as shown in Figure E1. The lower-limit depth of 1,000 m was fixed as the horizontal gradient of σ_0 is weak below this depth. This would have impacted the accuracy in the determination of Dc. From the 66 profiles, we computed mean values of this distance equal to 16 km associated with an STD of 8 km.

Figure 12 shows the Θ, SA, and σ_0 anomalies of RecAR as well as the Brunt Väisälä frequency squared (N^2). Such reconstruction clearly shows a dual core structure for RecAR. This is particularly discernible from the two low stratification layers in Figure 12d. The anomalies are important as they materialize the eddy content and transport of properties, such as heat and salt. The upper core lies at 350 m with peak anomalies of 3.7 °C, 0.56 g kg^{-1}, and −0.35 kg m^{-3} for, respectively, conservative temperature, absolute salinity, and potential density. The lower core lies at a depth of around 550 m and is characterized by anomalies of 4.4 °C, 0.62 g kg^{-1}, and −0.31 kg m^{-3}. The anomalies of conservative temperature and absolute salinity are more intense within the lower core but, due to their inverse effect on density, the density anomalies are nearly equal for both cores.

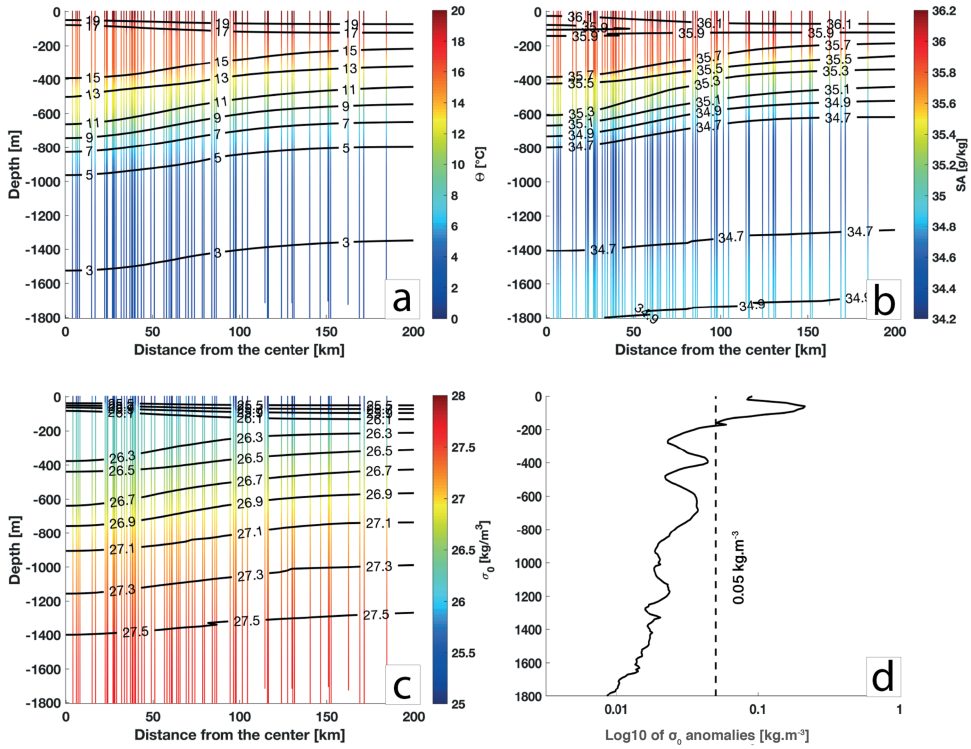

Figure 11. Superposition of the observed (background color) and the reconstructed (black contours) Agulhas Ring of the (a) conservative temperature (Θ), (b) absolute salinity (SA), (c) *potential density* (σ_0), and (d) root-mean-square error between the observed σ_0 anomalies and the reconstructed values computed at each depth.

In order to estimate the three-dimensional velocity structure (i.e., $V(r,z)$) for RecAR, we use the nonlinear thermal wind equation 7 (e.g., Ioannou et al., 2017):

$$\frac{1}{r}\frac{\partial V^2}{\partial z} + f\frac{\partial V}{\partial z} = \frac{-g}{\rho_0}\frac{\partial \rho}{\partial r}. \tag{7}$$

To solve this partial differential equation, the velocity field is set to 0 at a depth of 1,800 m (i.e., V(r,z = −1,800) = 0). The resulting velocity field is shown in Figure 13a. The maximum value of the azimuthal velocity is equal to 31 $\times 10^{-2}$ m s^{-1}. It is located at a depth of 200 m and at a distance of 63 km from the eddy center. This value is very close to the mean maximum speed radius, R_{Vmax} = 64 km, estimated from the surface geostrophic velocity field during the 12 month period. In comparison to the grid resolution of ADT maps (1/4°), this difference in values is negligible.

In order to estimate the limits of the volume of water trapped within RecAR, we followed Flierl (1981) defining the volume of trapped water in an eddy as the envelope of depths enclosed within the outer eddy limit where the azimuthal speed is equal to or higher than the translating speed of the eddy. For that, we computed the translation speed of the eddy during the period of time of interest using the trajectory of the geometrical center of the eddy computed by TOEddies. The resulting median translation speed is 5.7 with an STD of 1.4 $\times 10^{-2}$ m s^{-1}.

We then identified the line delimiting the trapped water inside RecAR (called separatrix here, following De Steur et al. (2004)) by hypothesizing that the eddy is circular and is moving at a constant speed. The black solid line in Figure 13a indicates the approximate location of the separatrix at each depth and the two black dashed lines delimit the STD (1.4 $\times 10^{-2}$ m s^{-1}) of the mean translation speed. The separatrix is located below a depth of 1,000 m and at less than ~100 km from the eddy center. It should be noted here that 1,000 m is the parking depth for most of the core Argo floats. The fact that the eddy is coherent at this depth explains why the Argo float No. 5902281 remained trapped within the structure for so long.

We also compared the steady horizontal velocity structure of RecAR with the eddy evolving surface geostrophic velocities derived from satellite altimetry. Figure 13b shows the various surface geostrophic velocity profile derived from satellite altimetry and provided by AVISO (in colors, starting in November 2012

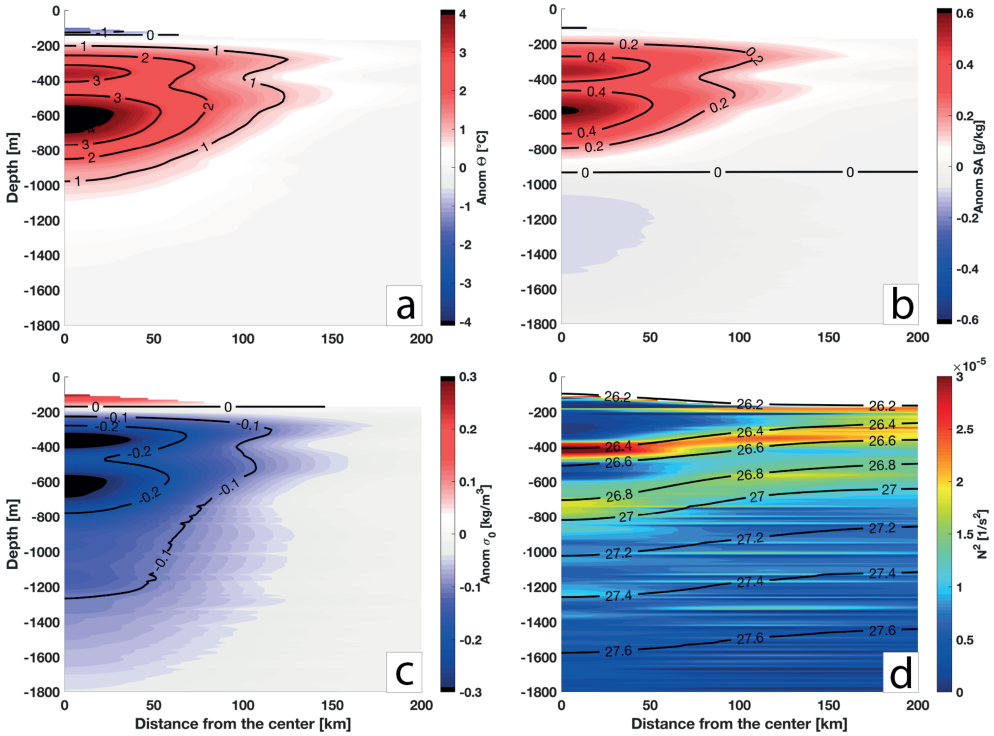

Figure 12. Anomalies of (a) conservative temperature (Θ), (b) absolute salinity (SA), (c) *potential density* (σ_0), and (d) Brunt Väisälä frequency squared (N^2) for the reconstructed Agulhas Ring. Contours in (d) are isopycnals of the reconstructed Agulhas Ring. The gray patch near the surface in each panel corresponds to the region above the isopycnal surface 26.2 kg m^{-3}, which marks the separation between the subtropical gyre upper warm waters and the eddy upper limit.

with the blue color and ending in October 2013 with the red color) as well as the velocity profile at a depth of 200 m (black solid line). The latter corresponds to the white dashed line in Figure 13a and depicts the position at which the azimuthal velocities reach a maximum. During the period of time in question, the V_{max} derived from satellite altimetry decreased with time from 35 $\times 10^{-2}$ m s^{-1} to 15 $\times 10^{-2}$ m s^{-1} while R_{Vmax} remained approximately constant (Figure 3a). Therefore, in less than a year, the surface geostrophic velocity corresponding to the eddy position dropped to half the value of the mean RecAR subsurface geostrophic velocity intensity. Given the large extent of the Agulhas Ring (both horizontally and vertically) and its intense thermohaline signature, we suggest that the observed decrease in the surface velocity is not due to a mechanism of dissipation of the eddy but to the decorrelation of the structure main core from the upper water layer attributable to its subduction during the Fall of 2012. This is confirmed by the hydrological anomalies near the ocean surface being of opposite sign to those in the eddy subsurface core, as suggested by Assassi et al. (2016) and Schütte et al. (2016). As a consequence, the surface layer has an inverse effect on the vertically integrated properties (such as dynamic height, the eddy geostrophic velocity, etc.) compared to that of the eddy at its core. This can explain, at least partially, the observed decrease in such variables observed since the subduction of the Agulhas Ring.

3.4. Integral Properties of the Subsurface Agulhas Ring

We used the separatrix and the 26.2 kg m^{-3} isopycnal surface to identify both the eddy lower (z_s) and upper (z_0) limits to compute the RecAR volume. This amounts to 7.1 $\times 10^{13} \pm$ 1.5 $\times 10^{13}$ m^3 where the confidence interval is computed using the STD of the eddy translation speed (as it impacts the volume integration). The temperature and salinity anomalies integrated between z_s and z_0 for both the Argo profiles and RecAR are presented in Figure 14. Here, again, a clear relationship appears between these values and the distance (Dc) from the eddy center. Moreover, the anomalies computed for RecAR and directly from the Argo profiles are in strong agreement, which supports our results and methodology.

$$HCA = 2\pi \int_0^{R_s} \int_{z_s}^{z_0} \rho C_p \Delta\Theta r d_r d_z, \tag{8}$$

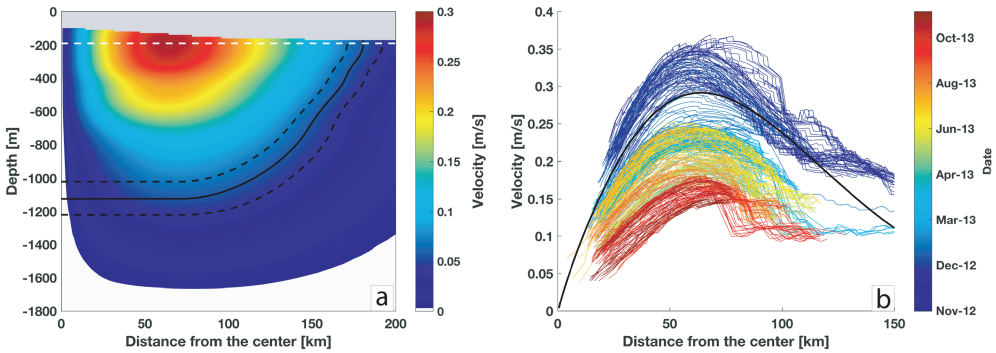

Figure 13. (a) Velocity field of the reconstructed Agulhas Ring computed from hydrographic data and (b) evolution of the geostrophic currents derived from satellite altimetry maps as a function of the distance from the center. The black line in (b) is the velocity derived from hydrographic data at −200 m (i.e., where this velocity is at its maximum). A dashed white line is added at this depth in panel (a). The black line in panel (a) corresponds to the separatrix where the velocity is equal to 5.7×10^{-2} m s^{-1} which is the median translation speed during the period November 2012 to November 2013. The dashed lines indicate the ± one STD ($\pm 1.4 \times 10^{-2}$ m s^{-1}) limits of the separatrix. The gray patch in panel (a) corresponds to the region above the isopycnal surface 26.2 kg m^{-3}, which marks the separation between the upper subtropical gyre waters and the upper limit of the eddy.

$$SCA = 2\pi \int_0^{R_s} \int_{z_s}^{z_0} \rho \Delta SA r d_r d_z. \tag{9}$$

We estimated the eddy anomalies of heat (HCA) and salt (SCA) from the temperature and salinity anomalies we computed for RecAR and by integrating equations 8 and 9 where C_p is the heat capacity, $\rho(r,z)$ the density, $\Delta\Theta(r,z)$ the conservative temperature anomalies in kelvin, and $\Delta SA(r,z)$ the absolute salinity anomalies of RecAR, whereas $R_s(z)$ is the radius of the separatrix. It is then possible to integrate, along the vertical, such anomalies to assess the total integrated HCA and SCA for RecAR. The values we obtained were, respectively, $2.5 \times 10^{20} \pm 1.3 \times 10^{19}$ J and $6 \times 10^{12} \pm 1.2 \times 10^{11}$ kg where ± indicates the STD.

To be able to compare to simpler estimates not depending on a precise determination of the eddy volume defined by the separatrix, we integrated the RecAR temperature and salinity anomalies from depths of 1,800 to 150 m over the 200 km area around the eddy center. The values we obtained were 2.9×10^{20} J for HCA and 4.8×10^{12} kg for SCA. The estimates obtained by the two approaches are very close for HCA whereas they differ significantly for SCA. This is very likely due to the presence of a negative patch of AS anomalies not taken into account in the estimates obtained from the first approach as this patch lies below the eddy trapping depth (Figure 12b).

Finally, the instantaneous volume, heat, and salt transport anomalies are computed following the method introduced by Olson and Evans (1986) and also used by Doglioli et al. (2007). These physical quantities are obtained by multiplying the integrated eddy properties with the translation speed divided by the diameter of the structure. They account for the transport generated by an eddy crossing an imaginary section. For the purposes of calculating transport values, the radius of the volume section was identified as that of the separatrix that reached the 26.2 kg m^{-3} isopycnal surface. This criteria led to a radius of 180 km. The resulting volume, heat, and salt transports STD are, respectively, 6 ± 0.5 Sv, 0.02 ± 0.004 PW, and $5.5 \times 10^5 \pm 1.4 \times 10^5$ kg^{-1}. These values are large as they correspond to the instantaneous transport of an Agulhas Ring. However, they cannot be used to compare directly with most estimates given in the literature as these assess the generic impact of Agulhas Rings by dividing the volume, heat, and salt contents of each eddy by the number of seconds in 1 year (e.g., Garzoli et al., 1999; van Ballegooyen et al., 1994). By using this generic approach, the transport of volume, heat, and salt would amount to, respectively, 2.2 Sv, 8.0×10^{-3} PW, and 2.2×10^5 kg s^{-1}.

4. Comparison with Agulhas Rings Identified in the Literature

For more than two decades, numerous Agulhas Rings have been sampled by in situ data. In this section, we compare the subsurface properties of RecAR with 27 different of those Agulhas Rings described in the literature (see Table 1 for a list of these studies). This database constitutes an important frame of reference from which to test the robustness of the properties and characteristics we derived for RecAR (as, e.g., the presence of MWs at its core, or its subsurface nature since crossing the Walvis Ridge). In the following

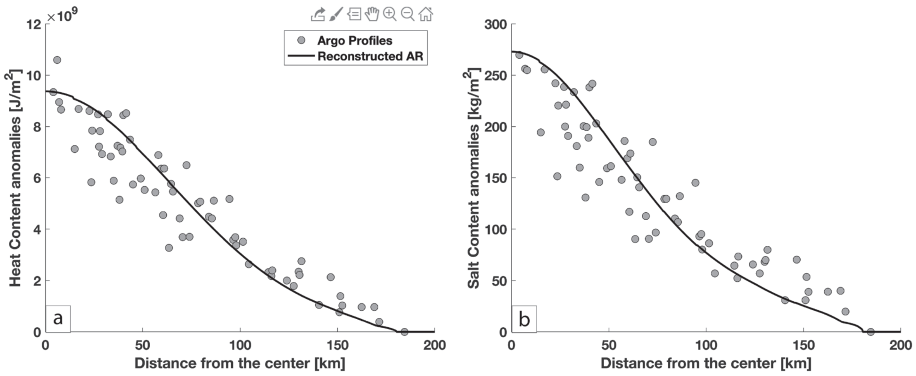

Figure 14. Anomalies of (a) heat content and (b) salt content as a function of the distance from the eddy center derived for both the reconstructed Agulhas Ring and the Argo profiles sampling the eddy. These values are obtained by integrating equations 8 and 9 vertically from the eddy separatrix up to 200 m.

section, we first introduce the general structure of the observed Agulhas Rings before focusing on MWs' properties, with an emphasis on those found within the rings. Finally, we compare estimates of their volume as well as heat and salt contents.

4.1. Agulhas Rings General Vertical Structure and Classification

The Agulhas Ring described in this study is characterized by two cores of MW that concentrate the essential fraction of the eddy anomalies when compared to surrounding waters. In this section, we wish to verify whether this is a common albeit not general vertical water mass organization for Agulhas Rings. Out of the 27 referenced eddies, 23 were sufficiently described in the literature to be used for the comparison (Arhan et al., 1999, 2011; Casanova-Masjoan et al., 2017; Duncombe Rae et al., 1992, 1996; Garzoli et al., 1999; Gladyshev et al., 2008; Gordon et al., 1987; Guerra et al., 2018; McDonagh et al., 1999; McCartney & Woodgate-Jones, 1991; Schmid et al., 2003; van Ballegooyen et al., 1994). We identified as single- or double-core MW eddies those Agulhas Rings whose vertical structure displayed one or two homogeneous layers thicker than 100 m and separated by at least two isotherms of θ<1 °C and two isohalines of PSU < 0.2°. Each of these eddies were observed during synoptic cruises. Thus, they can be associated with a single center position, whereas the Agulhas Ring we analyze in this study has been sampled by various Argo profiles along a segment of its trajectory. Hence, it cannot be associated with a single position for its center. Consequently, hereinafter we use the averaged location of the segment of trajectory that we reconstructed as the position of RecAR.

Of the 24 Agulhas Rings analyzed (i.e., 23 from the literature and our own RecAR), all show at least one core of water with homogeneous hydrological properties, and four exhibit two such cores (see Figure 15a). Three of them were observed northwest of the Cape Basin, as was the case for RecAR, whereas the other was found inside this basin.

We also tried to distinguish, among the documented rings in the literature, those eddies that could be considered surface intensified and those (if any) that could be described as subsurface structures. The classification of eddies as surface or subsurface intensified structures is difficult from sparse CTD data. Indeed, due to air-sea interactions, a seasonal thermocline can appear near the ocean surface that might not, necessarily, isolate the eddy structure from the mixing layer during the entire annual cycle. Consequently, we have characterized eddies as subsurface intensified according to their shape. Following the schematic view presented by Assassi et al. (2016), subsurface intensified Agulhas Rings are defined as those anticyclones showing a lenticular shape with isopycnals on the top of the homogeneous core that are shallower at the eddy center and deeper at the eddy edge. Among such categorization of subsurface eddies, an exception is the eddy described in Guerra et al. (2018) whose structure was derived from a single profile. The first homogeneous core documented by Guerra et al. (2018) lies below 100 m. We associated it with a subsurface eddy, even if the horizontal structure of the eddy was not provided.

Of the 23 Agulhas Rings we selected from the literature, 10 of them (i.e., ~40% are subsurface intensified and are indicated with red markers in Figure 15b. In general, they align along the southeast-northwest diagonal in the center of the Cape Basin following the main Agulhas Rings route (e.g., Dencausse et al., 2010; Guerra et al., 2018; Laxenaire et al., 2018) whereas the surface intensified ones (in blue in Figure 15b) lie closer to the Agulhas Retroflection area and the continental slope of the Cape Basin. It is worth noting that the eddy

Table 1
List of All Studies Having Described at Least One Agulhas Ring in Depth During Dedicated Oceanographic Cruises

Article	Number of eddy
Gordon et al. (1987)	2
Cartney and Woodgate-Jones (1991)	1
Duncombe Rae et al. (1992)	1
van Ballegooyen et al. (1994)	4
Duncombe Rae et al. (1996)	6
Arhan et al. (1999)	3
Garzoli et al. (1999)	3
McDonagh et al. (1999)	2
Schmid et al. (2003)	1
Gladyshev et al. (2008)	1
Arhan et al. (2011)	1
Casanova-Masjoan et al. (2017)	1
Guerra et al. (2018)	1
Total	27

Note. It should be noted here that the list is limited to those Agulhas Rings sufficiently documented in the referenced studies.

observed by Arhan et al. (2011) while it was sitting above the Agulhas Ridge is also a surface intensified eddy associated with a surface mixed layer depth of ~30 m which capped a homogeneous layer of more than ~500 m of thickness (Arhan et al., 2011). Consequently, Arhan et al. (2011) characterization of this eddy as surface or subsurface is not straightforward. Similarly, the eddy described by Casanova-Masjoan et al. (2017) shows a lenticular shape in salinity but not in temperature nor in potential density (see Figure 3 in Casanova-Masjoan et al., 2017). Consequently, its classification as either a surface or subsurface eddy was also difficult. As its upper part lies very close to the ocean surface we categorized it as a surface intensified eddy. Three of the subsurface intensified eddies showed a double core with homogeneous properties and with a very similar vertical structure to RecAR. Like RecAR, two of them were found in the Southeast Atlantic.

In conclusion, we categorized the whole set of Agulhas Rings in four different categories according to the number of cores with homogeneous properties and whether they were surface intensified eddies or not.

4.2. Agulhas Rings Mode Waters

The two-dimensional axisymmetric structure of RecAR has two distinct cores with homogeneous water properties that fall into the MWs category. As these waters are responsible for the majority of the eddy heat and salt anomalies (with reference to the environmental waters), it is important to compare the RecAR properties with similar structures documented in the literature in order to estimate the commonalities of their properties as well as their origins. Of the 27 Agulhas Rings identified in previous studies (see Table 1) that show one or two cores of MW, five (i.e., ~20%) have their upper limit shallower than 50 m. For these five eddies, the subsurface homogeneous layer has been described by the authors of the relevant studies as a deep mixed layer. Deep homogeneous layers are indeed thought to be the first and necessary phase of MW formation (e.g., Alfultis & Cornillon, 2001; Joyce, 2012; Sato & Polito, 2014). These deep mixed layers have been shown to be common in eddies, and they appear to occur more in anticyclones than in cyclones (Kouketsu et al., 2012; Sato & Polito, 2014).

The hydrological properties of the documented Agulhas Ring MW cores are presented in Tables G1 and G2. The position at which these eddies were sampled and their θ-S characteristics are shown, respectively, in panels (a) and (b) of Figure 16. Figure 16b shows that their properties range from 25.4 to 26.8 kg m^{-3} in σ_0, from 12 to 19 °C in potential temperature, and from 35.08 and 35.75 in (practical) salinity units.

As discussed in the Introduction, various MWs are described in the literature. We have summarized their properties in Table F1. Even if very similar, they all show small property differences. Recently, de Souza et al. (2018) discussed a possible contribution of distinct MWs to South Atlantic Central Water (SACW). However, as they decomposed SACW by MW contribution, the specific hydrological properties of the various SATMWs cannot be derived directly from that publication.

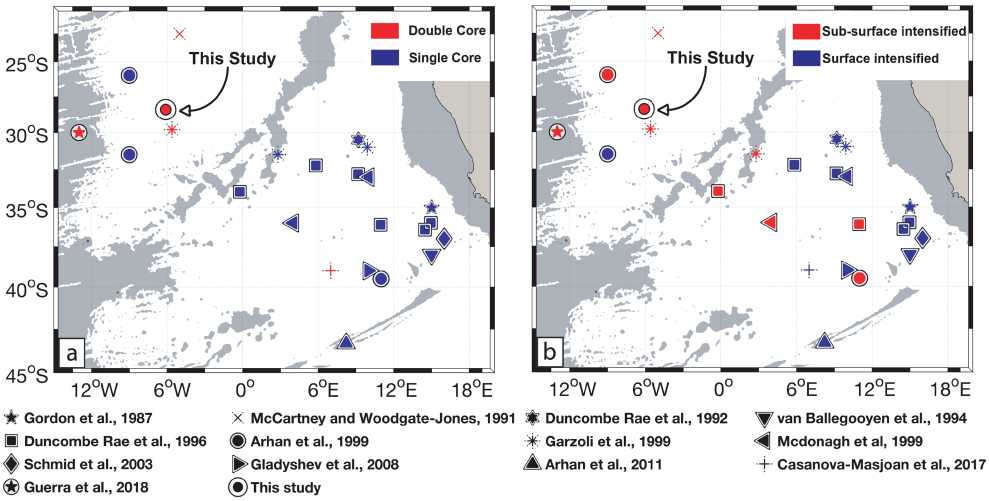

Figure 15. Number of (a) cores and (b) type of internal structure of the Agulhas Rings described in the literature. Each article is associated with a unique marker type. The gray shading patches in (a) represent water depth shallower than 3,500 m in the ETOPO2 data set (Smith & Sandwell, 1997).

Here, we compared the whole set of Agulhas Ring MWs (that includes RecAR and all those found in the literature) to Sato and Polito (2014) SATMWs. Figure 16 presents the Sato and Polito (2014) SATMWs' hydrological distributions as areas shaded in blue (SASTMW2) and green (SASTMW3). We do not consider here SASTMW1, which is only found west of 30°W whereas SASTMW2 and SASTMW3 occupy the eastern South Atlantic sector. SASTMW2 and SASTMW3 are separated by the 35°S parallel (see Figure 4 in Sato and Polito (2014)).

Agulhas Ring MW core properties fall in the range of SASTMW2 and SASTMW3. Moreover, more than 50% of these Agulhas Ring MW cores have properties within the generic SASTMW characteristics (see Table F1). In particular, nearly all the surface Agulhas Rings that have a single MW core (in black) are in the range of SASTMW2, whereas the whole set of subsurface Agulhas Rings with a simple MW core (green) fall in the SASTMW1 category. The only exception is the eddy described by Arhan et al. (2011), which shows a particularly thick homogeneous layer capped by a narrow surface layer. We identified it as a surface intensified eddy as the surface layer was only 30 m thick. However, this eddy, observed by the 2008 GoodHope cruise in late February, was clearly at the beginning of a phase described as a subduction by Arhan et al. (2011) as the eddy disappeared from the altimetry a few months later (at the beginning of April 2008, Arhan et al., 2011). Given the size and energy of this Agulhas Ring, it is improbable that it simply dissipated so quickly.

If we look at the spatial organization of single MW core Agulhas Rings in Figure 16a, we see that those that are surface intensified mainly lie near the African continental slope covering the eastern part of the Cape Basin. The subsurface ones, on the other hand, are essentially found in the central part of the basin, along the Agulhas Ring central path (Laxenaire et al., 2018).

Double-core MW Agulhas Rings have a simpler distribution. Most (4) subsurface double-core MW rings were observed north/northwest of the Cape Basin. That described by McCartney and Woodgate-Jones (1991) shows SASTMW2 characteristics, whereas the others three (Garzoli et al. (1999), Guerra et al. (2018) and RecAR) have properties falling in both varieties of SASTMW (see Figure 16b). Only one surface double-core eddy was identified in the literature so far (by Casanova-Masjoan et al. (2017)) lying in the center of the Cape Basin. The MW cores of this show both, SASTMW2 and SASTMW3 properties.

Arhan et al. (1999) and Arhan et al. (2011) have suggested that Agulhas Ring hydrological properties are intimately linked to their history. Indeed, these studies have suggested that the route undertaken by these eddies (northern, central, or southern according to Dencausse et al. (2010)), the time they spend within the subantarctic regions, and whether they experience a wintering or not are all factors that determine the water properties of the upper 1,000 m of these structures, mediated by strong air-sea interactions and mixing with environmental water. This might explain why, even if some correspondence between geographical regions and Agulhas Ring characteristics appear, there seems not to be a clear pattern. On the other hand, Garzoli et al. (1999) and Gladyshev et al. (2008) have suggested that Agulhas Rings displaying a multiple core

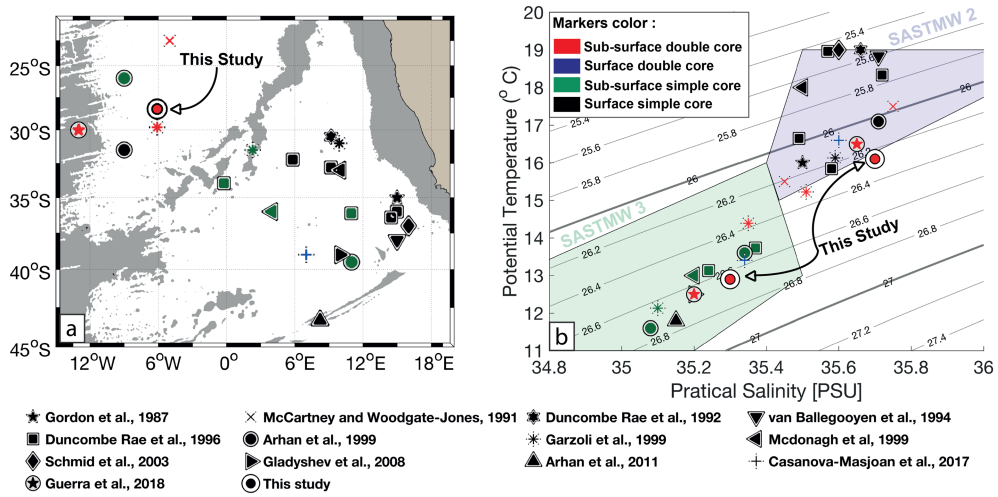

Figure 16. (a) Position and (b) hydrological properties in the mode water cores of the Agulhas Rings described in the literature. Each study discussing one or more of these eddies is associated with a specific marker, and the color corresponds to a particular type of eddy. Double-core mode water eddies have two similar markers. The gray shaded patches in (a) represent water depth shallower than 3,500 m in the ETOPO2 data set (Smith & Sandwell, 1997). The background lines in (b) represent isopycnals of potential density anomalies referenced to the surface pressure (σ_0). The blue and green shaded patches highlight the hydrological properties of, respectively, SASTMW2 and SASTMW3 as described by Sato and Polito (2014).

structure might be explained either by the merging of two rings with distinct histories or by two consecutive mode water formations during consecutive years.

Our study cannot completely explain the origins and diversity of Agulhas Ring MW properties and structure. Indeed, while the formation of the upper MW core was well captured by the profiles achieved by Argo float No. 5902281 during the time it was trapped within the eddy core, we do not have any information on the MW ventilation of the second and deeper one. The whole set of profiles that sampled Segments 1, 2, and 3 before they merged into Segments 4 and 5 (see Figure 2) did not sample the eddy structures close to the center so they cannot be assumed to characterize the inner eddy vertical structure. It should be noted that Segment 1 spent an entire winter south of 40°S, in the strong westerlies blowing in the subantarctic region, before merging with Segment 4 to form Segment 5. Segment 1 is very close, albeit it crossed the Walvis Ridge slightly north of the eddy observed by Arhan et al. (2011). This could explain the fact that both eddies display SASTMW2 characteristics but that the deeper core of RecAR is warmer and saltier than the homogeneous layer of the eddy discussed by Arhan et al. (2011), suggesting that RecAR underwent less intense air-sea interactions. Other published studies have suggested that MWs observed within Agulhas Rings are or might derive from modified (Indian) SAMW (e.g., Arhan et al., 1999; Gladyshev et al., 2008) or Subtropical Indian MW (de Souza et al., 2018). However, the definitions of these two MWs are not precise (see Table F1), and this prevents any clear conclusion. We can merely suggest that Agulhas Rings are large coherent structures advecting, south of Africa, Agulhas Current waters (i.e., Subtropical Indian waters). These waters are transformed along the way by ocean-atmosphere interactions. As suggested by Arhan et al. (2011), these exchanges, when occurring during winter, give rise to episodes of intense convection that are accompanied by lateral mixing with environmental water. Indeed, the large cooling and freshening of the homogeneous layer waters can be explained only by taking into account both processes. Moreover, the more intense the convection, the larger the mixing and therefore the greater the cooling and freshening. This can elucidate why the eddy observed by Arhan et al. (2011) southward of Segment 1's actual trajectory showed lower temperature and salinity than RecAR.

The precise processes involved in the formation of relatively deep mixed layers within Agulhas Rings and how these layers transform into MW cores have not been directly observed. However, by using very high-resolution numerical simulations, Capuano et al. (2018) showed that submesoscale instabilities (of different type) are responsible for both deep mixing layer formation during winter and the upper-layer restratification during summer as discussed in section 2.2 describing possible mechanisms of subduction. Moreover, this type of instability leads to mixing layer water subduction and the formation of a local variety of mode water that the authors defined as Agulhas Ring Mode Water (ARMW) and whose properties depend on the eddy history. These numerical results, as well as our analyses on the observed Agulhas Ring

MW properties, would suggest that MWs found in Agulhas Ring cores are formed within these eddies and not a regional variety of SASTMW corresponding to a more classical and larger-scale definition of water mass subduction. Yet from the in situ data we have analyzed, we are not able to reconstruct the entire evolution of RecAR, neither are we able to demonstrate unequivocally that ARMWs are the same water masses as SASTMW2 and SASTMW3, nor that they can be found only within eddies.

4.3. Agulhas Rings Volume Transport, and Heat and Salt Contents

Table 2 presents the estimates of the volume as well heat and salt content anomalies for 17 of the 27 Agulhas Rings found in the literature for which at least one of these values was provided by the authors of the studies in question. When the authors give more than one value for these variables for one eddy, we only provide those estimates computed using the closest boundaries of integration to ours.

The average Agulhas Ring volume, HCA, and SCA in the literature are, respectively, $3.4 \times 10^{13} \pm 1.6 \times 10^{13}$ m^{-3}, $1.0 \times 10^{20} \pm 0.7 \times 10^{20}$ J, and $5.2 \times 10^{12} \pm 3.6 \times 10^{12}$ kg. Hence, RecAR proves to be one of the strongest and largest Agulhas Rings ever observed. The estimated volume and HCA are more than double that of the Agulhas Ring documented values, and the SCA is slightly higher than their average.

All rings, with the exception of RecAR and two others (McCartney & Woodgate-Jones, 1991; Garzoli et al., 1999), were found in the Cape Basin. It might therefore be possible that the large values of RecAR for both HCA and SCA are due to a lateral mixing with surrounding waters. However, the fact that the waters trapped within the eddy show different properties from the environment and the MW cores are similar to those found in other Agulhas Rings gives us confidence that RecAR is a coherent mesoscale eddy advecting modified Indian waters into the South Atlantic. Beyond these conjectures, we can compare assessments of these integrated properties for RecAR and the rings documented in the literature by using the same approach as in the related articles. The results are presented in Table H1 where the values given in the articles are expressed as a percentage of the values for the same variables obtained for RecAR. This comparison shows that, even if we do not consider the upper 200 m of the water column for RecAR, it still results in the largest volume. RecAR is also one of the rings with the highest hydrological anomalies, higher than all but 2 and 4 of the other 16 for, respectively, RecAR HCA and SCA. However, these rings were observed close to the Agulhas Retroflection area.

5. Summary and Conclusions

We have analyzed the evolution of a long-lived Agulhas Ring during 1.5 years of its lifespan by simultaneously using a new eddy tracking algorithm (TOEddies) applied to satellite altimetry maps and Argo floats to uncover the eddy's hydrological properties. This eddy was sampled by a large number of Argo profiles (71) between the northern region of the Cape Basin and the Mid-Atlantic Ridge, similarly to the eddies discussed by Souza et al. (2011) and Nencioli et al. (2018). In particular, one of the Argo floats (No. 5902281) remained trapped within the eddy core for 14 months (from October 2012 to November 2013), which provided a vertical snapshot of the eddy every 10 days. We also selected all additional Argo profiles lying at less than 200 km from the eddy center. However, we made a careful distinction between the profiles sampling the eddy within its boundaries and those characterizing the environment. This was possible as the TOEddies method automatically computes, for every detected eddy, its outer and characteristic contours together with the evolution of its surface properties.

The eddy we discussed in this study corresponds to a segment of an Agulhas Ring main trajectory (according to the definition of Laxenaire et al. (2018)) that has been tracked by TOEddies for 4 years and 7 months (from January 2011 to July 2015). This segment was generated in the Cape Basin by the merging of three different Agulhas Rings. Along this segment the eddy proved to be particularly coherent in its shape whereas its surface ADT anomaly, velocity, and |Ro| decreased with time, as previously observed for other rings (e.g., Byrne et al., 1995; Guerra et al., 2018; Laxenaire et al., 2018; Schouten et al., 2000).

The subsurface observations of the eddy were characterized by two distinct periods: one in austral winter, during which the mixing layer in the eddy deepened significantly, and a second in austral summer, during which the upper hydrological core of the eddy subsided while propagating west. We showed that the eddy, when capped by surface warmer layers, is characterized by negative SST anomalies that support, according to Assassi et al. (2016), its characterization as a subsurface intensified eddy. This study represents, to our knowledge, the first Lagrangian evidence of the subduction of an Agulhas Ring. This result is supported by previous observations of a subducted Agulhas Ring (Arhan et al., 1999) and numerical studies by Herbette et al. (2004). However, from the data we have analyzed, we cannot infer precisely the mechanism

Table 2
Integrated properties of Agulhas Rings Described in the Literature

Article	Eddy	Volume (m^3)	HCA (J)	SCA (kg)	Reference
McCartney & Woodgate-Jones (1991)	Eddy	3.6×10^{13}			Trap 5×10^{-2} m s^{-1}
van Ballegooyen et al. (1994)	A3	4.31×10^{13}	1.5×10^{20}	8.74×10^{12}	T > 8 °C
van Ballegooyen et al. (1994)	A4	3.94×10^{13}	2.36×10^{20}	13.1×10^{12}	T > 8 °C
van Ballegooyen et al. (1994)	A5	1.53×10^{13}	0.73×10^{20}	4.35×10^{12}	T > 8 °C
van Ballegooyen et al. (1994)	A6	2.45×10^{13}	1.06×10^{20}	4.59×10^{12}	T > 8 °C
Duncombe Rae et al. (1996)	B1-1		0.19×10^{20}	1.21×10^{12}	800 m
Duncombe Rae et al. (1996)	B2-1		0.24×10^{20}	1.52×10^{12}	800 m
Duncombe Rae et al. (1996)	B2-2		0.57×10^{20}	3.8×10^{12}	800 m
Duncombe Rae et al. (1996)	B2-3		0.55×10^{20}	3.72×10^{12}	800 m
Duncombe Rae et al. (1996)	B2-4		0.42×10^{20}	1.67×10^{12}	800 m
Duncombe Rae et al. (1996)	B3-1		0.6×10^{20}	3.88×10^{12}	800 m
McDonagh et al. (1999)	R1	1.5×10^{13}	0.39×10^{20}	2.43×10^{12}	T > 10 °C
McDonagh et al. (1999)	R2	4.7×10^{13}	0.44×10^{20}	2.71×10^{12}	T > 10 °C
Garzoli et al. (1999)	R-1	2.8×10^{13}	1.33×10^{20}	8×10^{12}	1,100 m
Garzoli et al. (1999)	R-2	4.18×10^{13}	1.31×10^{20}		1,100 m
Garzoli et al. (1999)	R-3	1.88×10^{13}	0.77×10^{20}		1,100 m
Schmid et al. (2003)	JAR	2.8×10^{13}	1.71×10^{20}	10.7×10^{12}	1,100 m
This study	RecAR	7.1×10^{13}	2.5×10^{20}	6.8×10^{12}	Trap 6×10^{-2} m s^{-1}

Note. The reference for the bottom limit of integration is given in the last column. The integrations are achieved either from an isotherm for a fixed depth or by identifying the coherent part of the eddy assessed, following Flierl (1981), as the volume of the eddy where eddy velocities are lower than the eddy drifting speed. The upper limit of integration is the surface for all eddies except RecAR, for which the integration is limited to $\sigma_0 = 26.2$ kg m^{-3}.

that acted to separate the coherent part of the eddy from the upper layers. Indeed, we document the presence of significantly different water masses in the Agulhas Ring compared with the environment. The upper-layer hydrological properties of the Agulhas Ring appear different from the environment, too, but they are also distinct from those of the eddy core below. This indicates a clear separation of the Agulhas Ring core from the surface, resulting in a less coherent upper-layer behavior that enables the Agulhas Ring and surrounding waters to mix (e.g., Wang et al., 2015), producing modified water of Indian-Atlantic origins. Hence, for the particular Agulhas Ring discussed in this study, it appears that the eddy still influences the velocity in the surface waters rather than being completely separated.

The transition from a surface to a subsurface intensified eddy concomitant with the trapping of a profiling float is of a great interest in light of the question about the ability of eddy detection methods to detect coherent eddies (e.g., Abernathey & Haller, 2018) from a surface field. In the same way as in previous studies (Nencioli et al., 2018; Souza et al., 2011), the TOEddies eulerian detection algorithm showed it could successfully identify and track a coherent eddy as it is able to trap a profiling float for more than 1 year. However, the observation of the subduction of the eddy enabled us to go beyond these results as it documented that a reduction in the eddy surface intensity is not associated with the global dissipation of the structure but with its subsidence in the ocean interior. Indeed, the subducted eddy conserves its size and properties, and the maximum geostrophic velocity seems to move, while subducting, from the ocean surface to a depth of 200 m. In this case, the velocities at the surface still satisfy the trapping water conditions of Flierl (1981) and Chelton et al. (2011). However, we might expect this to not always be the case for the water column encompassing the surface layer and the full structure of the eddy at depth. This would result in an incoherent eddy-like behavior in the surface layer while the deeper layers of the eddy continued to behave as a coherent structure. Moreover, as the surface geostrophic velocity decreases, we can expect the signal-over-noise ratio to increase in satellite altimetry maps. This ratio is particularly important for Lagrangian eddy detection techniques (e.g., Abernathey & Haller, 2018; Beron-Vera et al., 2013) and is very sensitive to absolute values of the surface velocities. Therefore, we advise caution when analyzing eddies' coherence from surface fields only and, in particular, when estimating the Agulhas Leakage achieved by Agulhas Ring (e.g., Wang et al., 2015, 2016). Indeed, our results suggest that Agulhas Ring can behave as a coherent structure, but mainly so within the subsurface layers.

Another possible consequence of the subduction process might be the formation of mode water layer cores. Indeed, the eddy we studied presented two cores of mode waters. One of these was very likely linked to the last winter convection as described by Capuano et al. (2018). A second one, located deeper, was probably linked to a merging of an Agulhas Ring that took, after being spawned by the Agulhas Retroflection, the Southern Route defined by Dencausse et al. (2010) and experienced more intense winter conditions.

Given the long-lasting coherence of the structure after subduction, which shielded the eddy from any further air-sea exchanges, we assumed it was steady and axisymmetric. This allowed us to reconstruct its three-dimensional hydrological vertical structure by fitting an alpha Gaussian function (e.g., Carton, 2001; Le Vu et al., 2018; Zeitlin, 2018). We defined the eddy thermohaline anomalies in relation to the surrounding environment. These anomalies turned out to be very intense and concentrated within the two mode water layers, and they concentrated the majority of the anomaly signal distinguishing this eddy from the surrounding South Atlantic waters. Our reconstruction is similar to the approach of Nencioli et al. (2018) who studied a different eddy. However, it differs in the choice of the variables of integration and in the definition of the eddy boundaries. Indeed, we carefully considered only profiles falling strictly within the eddy limits (lateral and vertical) with a view to accurately representing the eddy thermohaline structure.

A comparison with 27 other Agulhas Ringdescribed in the literature from oceanographic cruises shows that we can subdivide them into surface and subsurface intensified rings. The surface intensified rings mainly lie in the Cape Basin, along the Southern Africa slope. Those located along the main ring path that occupies the central part of the Cape Basin (Laxenaire et al., 2018) are predominantly subsurface intensified eddies. Moreover, the rings for which we have found in the literature a vertical section of their thermohaline properties are all characterized by the presence of at least one core of mode waters. Some of them show two mode water cores (including the eddy we focus on in this study). For these, all but one are located in the South Atlantic, north of the Cape Basin. Hence, the results of the comparison suggest that the subsurface eddy we reconstructed in this work, which is composed of two homogeneous cores, is not an exception. Moreover, this analysis provides indications that Agulhas Rings follow a geographical pattern according to their history and water mass properties. Such a distribution needs to be investigated further from updated data, complementary modeling studies, and by applying reproducible quantitative methods.

The mode waters found in Agulhas Rings show very variable properties that fall within the range of two varieties of SASTMW (Sato & Polito, 2014) and in the upper (warmer and saltier) range of SAMW (McCartney & Woodgate-Jones, 1991). However, the continuity of their θ-S properties would rather suggest that these eddies are associated with one specific variety of mode water formed within Agulhas Rings during the austral winter (the so-called ARMW as suggested from modeling studies by Capuano et al. (2018)) and not to different types of mode waters formed remotely. Indeed, south of Africa the ocean is submitted to intense wind forcing and buoyancy exchanges that affect in particular the warm and salty Agulhas Current and Agulhas Rings (e.g., Arhan et al., 1999, 2011; van Ballegooyen et al., 1994). The assorted properties observed for ARMWs might be due to the different amplitude of such air-sea fluxes as these vary according to the path undertaken by the rings, as well to the synopticity of the atmospheric forcing that can vary from 1 week to another as well as 1 year from the following, or according to the time the rings spend in the area as they can be blocked for several months by the interaction with the local topography (e.g., Arhan et al., 1999; Arhan et al., 2011). Yet our study cannot assess whether the formation of the observed mode waters are restricted to Agulhas Rings only nor can it define the origin of the observed mode waters for the double-core rings. The latter might indeed be the result of convection within an eddy during two consecutive winters or of the merging of two rings that took different routes and underwent different weather conditions (Garzoli et al., 1999). Also, the deeper mode water core could be a remnant of SAMW advected within the Agulhas Current from the Indian Ocean and already present in the eddy at the moment it was spawned from that current.

We calculated the geostrophic velocity of the reconstructed eddy from the nonlinear thermal wind relation. The maximal value of the azimuthal velocity (0.3 m s^{-1}) was found at 200 m and had the same radius as the speed radius derived from satellite altimetry. The surface maximum azimuthal velocity was more intense (up to 0.35 m s^{-1}) than its subsurface expression from November 2012 to January 2013. After this period it decreased steadily to reach 0.15 m s^{-1} at the end of the Argo float No. 5902281 observing period. This is a consequence of the eddy subduction that implies at least a partial disconnection of the eddy from the ocean surface. Our analysis suggests that the eddy extended, after subduction, from a depth of 200–1,200 m. We estimated its volume at $7.1 \times 10^{13} \pm 1.5 \times 10^{13}$ m^{-3}. The heat and salt anomalies transported

by the eddy amounted to, respectively, 4 °C and 0.6 g kg^{-1} at a depth of 600 m and the total integrated heat content anomalies (HCA) and salt content anomalies (SCA) were estimated at 2.5 $\times 10^{20} \pm$ 0.1 $\times 10^{20}$ J and 6.8 $\times 10^{12} \pm$ 0.1 $\times 10^{12}$ kg, respectively. Both the volume and the hydrological anomalies proved to be particularly large when compared with comparable estimates for Agulhas Rings found in the literature. Only Agulhas Rings close to the Agulhas Retroflection show comparably large integrated hydrological anomalies (e.g., Arhan et al., 1999, 2011; Schmid et al., 2003; van Ballegooyen et al., 1994).

Our analysis sheds light on the complex evolution of Agulhas Rings that split and merge, undergo intense ventilation, and subduct but remain intense while crossing the South Atlantic basin. They advect very large quantities of water, heat, and salt from the Indian Ocean. South of Africa, Agulhas Ring waters are (at least partially) modified by winter convection that produces thick cores of mode waters. It is in these mode water cores that the strongest heat anomaly of these intense eddies seems to reside, when they are advected in the South Atlantic Ocean. This, together with the numerous eddy merging and splitting occurrences, strongly suggests that the use of exclusively satellite altimetry maps to characterize the coherence of eddies has limitations and that coupling with Argo profiles is very useful.

Appendix A: Argo Profiling Float Trajectories

The trajectories of the Argo floats trapped in the AR studied here are shown in Figure A1.

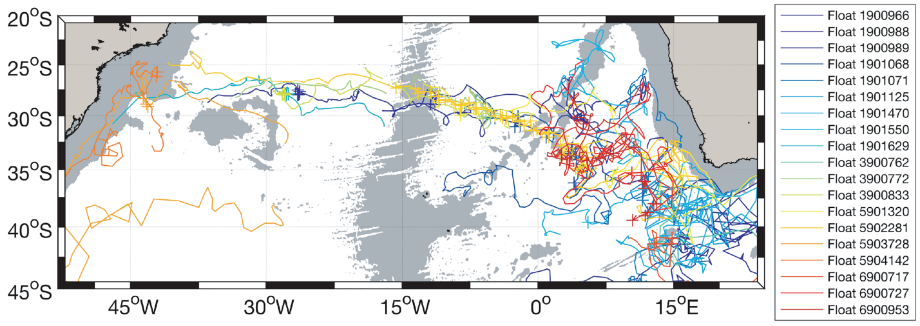

Figure A1. Trajectories and names of the profiling floats that sampled the AREN of interest. The profiles used in this study are marked by crosses.

Appendix B: Bathymetry Below the Fifth Trajectory Segment

The bathymetry interpolated from ETOPO2 along the fifth trajectory is shown in Figure B1.

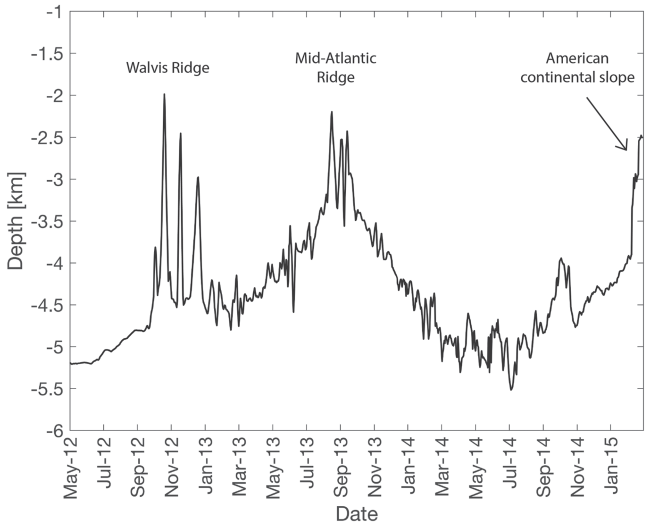

Figure B1. Bathymetry below the fifth trajectory segment of the Agulhas Ring main trajectory studied in this work from the ETOPO2 data set (Smith & Sandwell, 1997).

Appendix C: SST Anomalies

The SST anomalies in the mooving frame of the Agulhas Ring is presented in Figure C1.

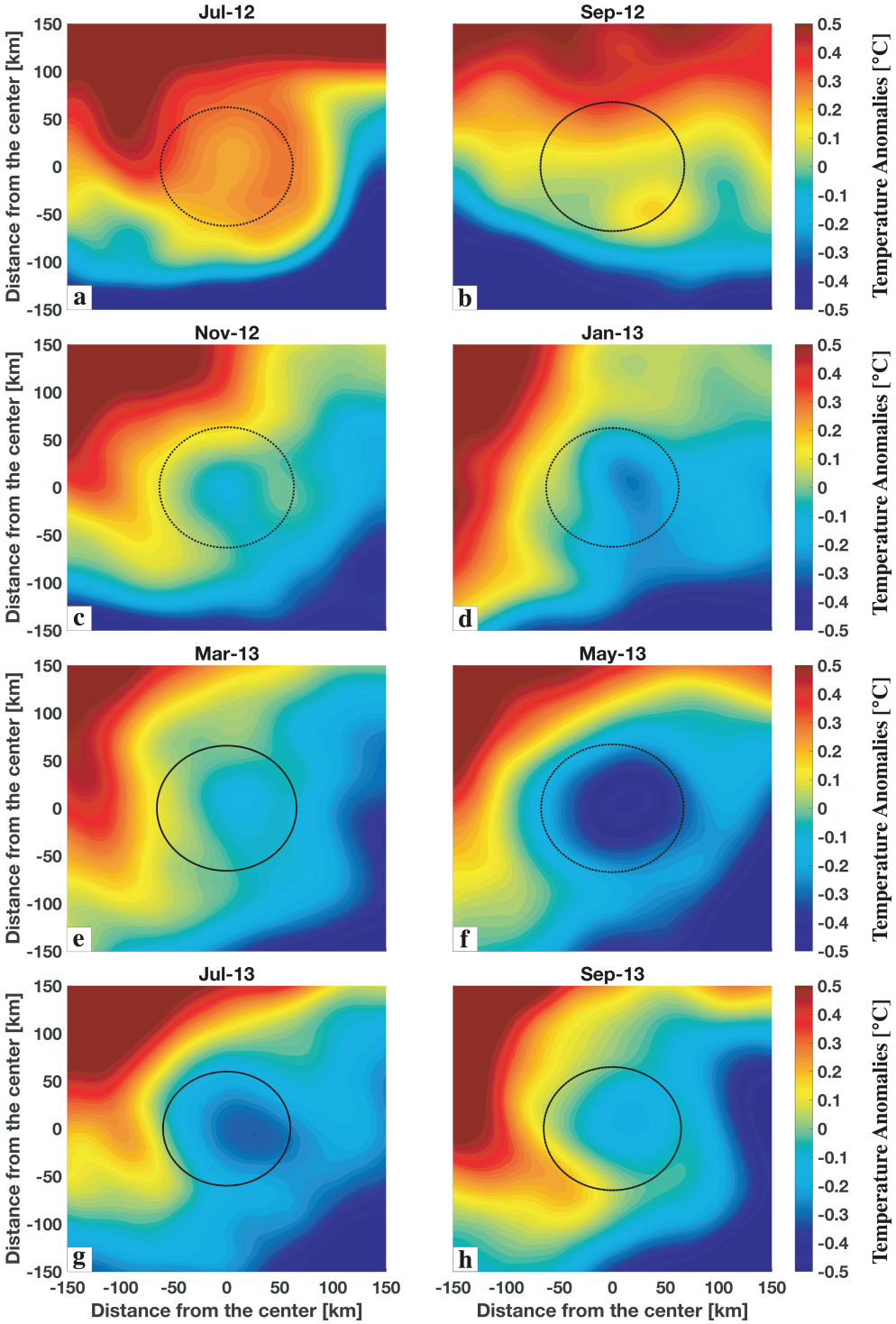

Figure C1. Monthly averaged SST anomalies in the moving reference frame of the fifth segment of the AREN interpolated from the ODYSSEA SST data set (Dash et al., 2012; Martin et al., 2012). These anomalies are computed by subtracting the mean SST in each panel from the SST values at each point.

Appendix D: Θ-SA Diagram

The T/S properties of the Argo profiles sampling the Fifth trajectory segment are presented in the Figure D1.

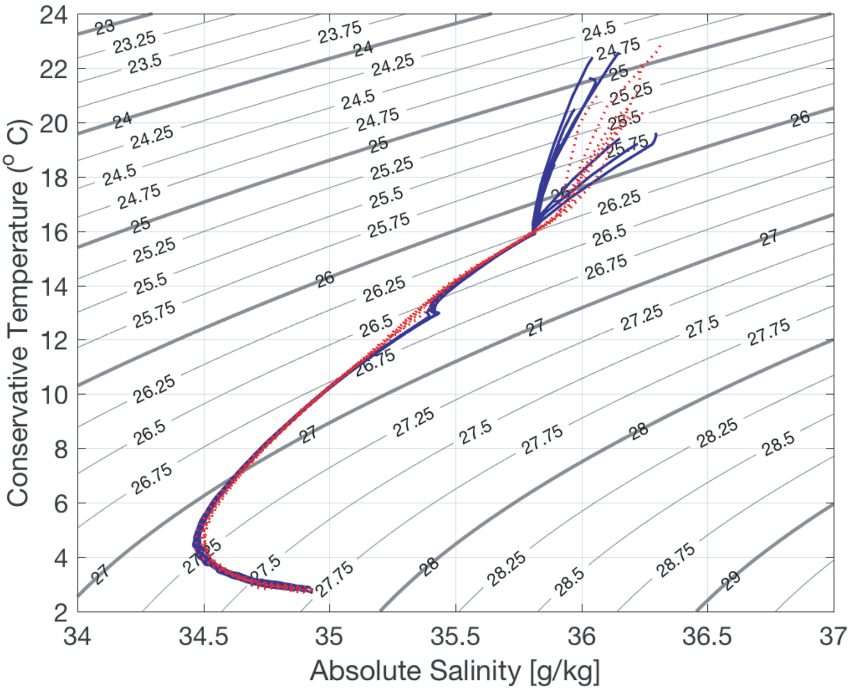

Figure D1. Θ-SA diagram of Argo profiles with a Dc < 25 km in red and those with a 150 < Dc < 200 km in blue sampling Segment 5 between November 2012 and November 2013.

Appendix E: Examples of Potential Anomalies Reconstruction

The reconstructed RecAR and independant Argo profiles at plotted at selected depth in the Figure E1.

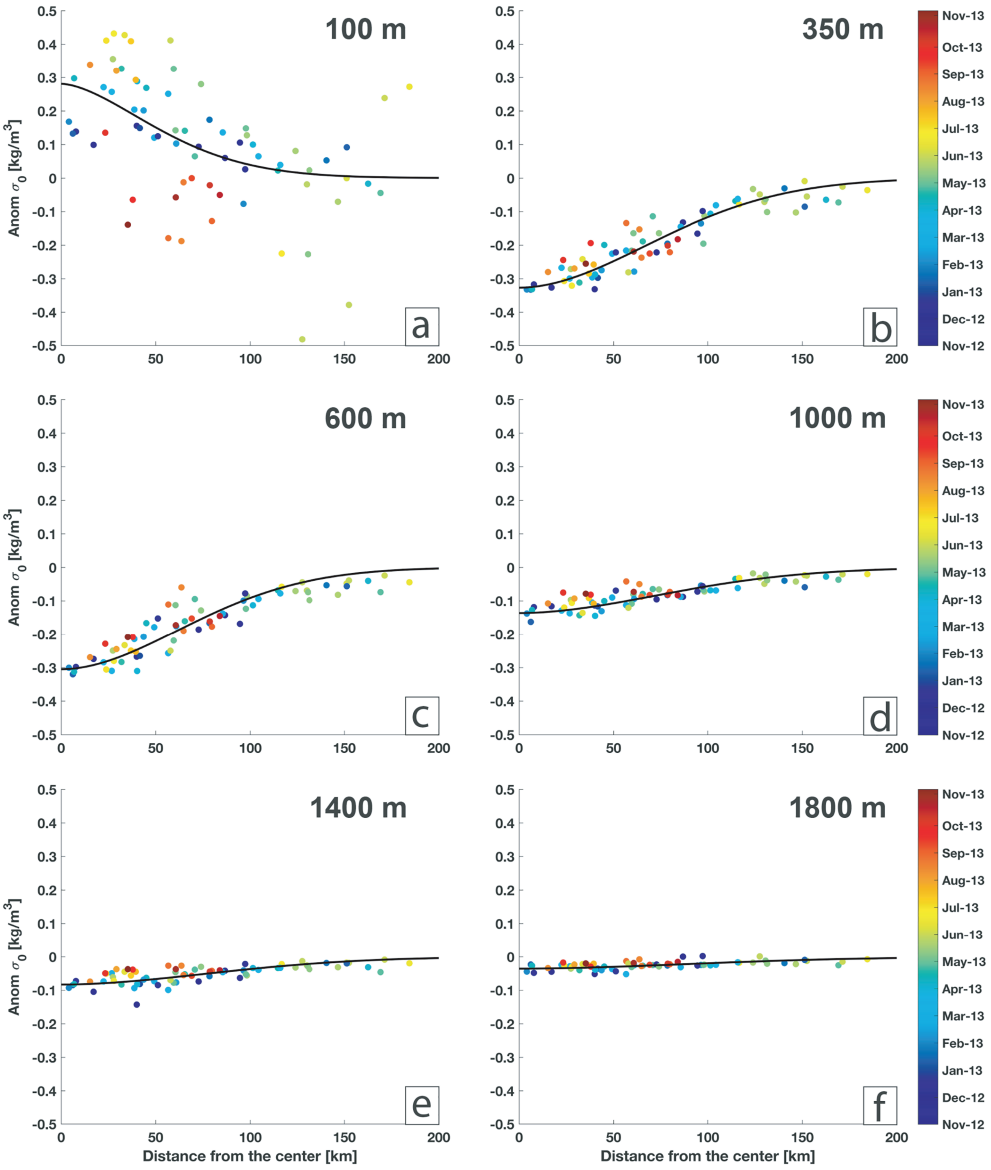

Figure E1. *Potential density anomalies (Anom σ_0)* derived from Argo observations (circles) and from the reconstructed Agulhas Ring (solid black lines) at six different depths as a function of the distance from the eddy center (Dc). The date for each observation is indicated by the color of the circles.

Appendix F: Hydrological Properties of Mode Waters Found in the South Atlantic as Described in the Literature

The Mode Water properties described by various authors in the region of interest are listed in Table F1.

Table F1
Hydrological properties Potential Temperature (θ in °C), Practical Salinity (S in PSU), and Potential Density (σ_θ in kg m^{-3}) of Mode Waters Found in the South Atlantic as Described in the Literature

Acronym	Full name	θ (°C)	PSU (psu)	σ_θ (kg m^{-3})	Reference
SAMW	Subantarctic MW	4–15	34.2–35.8	26.5–27.1	McCartney (1977, 1982)
SASTMW	South Atlantic STMW	12–18	35.2–36.2	26.2–26.6	Provost et al. (1999)
SAESTMW	South Atlantic Eastern STMW	15–16	35.4	26.2–26.3	Provost et al. (1999)
SASTMW1	South Atlantic STMW 1	15.0 ± 0.9	35.6 ± 0.2	26.4 ± 0.1	Sato and Polito (2014)
SASTMW2	South Atlantic STMW 2	16.7 ± 0.9	35.7 ± 0.2	26.1 ± 0.1	Sato and Polito (2014)
SASTMW3	South Atlantic STMW 3	13.2 ± 0.9	35.2 ± 0.2	26.5 ± 0.1	Sato and Polito (2014)
$STMW_{18}$	STMW $\theta = 18$	18 ± 0.56	35.8 ± 0.11	25.9	de Souza et al. (2018)
$STMW_{14}$	STMW $\theta = 14$	14 ± 0.53	35.40 ± 0.01	26.5	de Souza et al. (2018)
$STMW_{12}$	STMW $\theta = 12$	12 ± 0.50	35.03 ± 0.14	26.6	de Souza et al. (2018)
SIMW	Subtropical Indian MW	17 ± 0.28	35.57 ± 0.54	26.0	de Souza et al. (2018)

Note. The standard deviations (STD) is provided using the ± symbol when it is explicitly supplied in the articles.

Appendix G: Hydrological Properties of the Agulhas Ring's Cores Described in the Literature

The hydrological properties of the Agulhas Ring cores described in the litterature are listed in the Tables G1 and G2.

Table G1
Properties of the Agulhas Ring Cores Described in the Literature

Article	Eddy core number	Depth (m)	Thickness (m)	θ (°C)	PSU (psu)
Gordon et al. (1987)	CTE.1	−230	200	16	35.5
McCartney and Woodgate-Jones (1991)	Eddy.1	−150	100	17.5	35.75
McCartney and Woodgate-Jones (1991)	Eddy.2	−250	100	15.5	35.45
Duncombe Rae et al. (1992)	Ring.1	−50	100	19	35.66
van Ballegooyen et al. (1994)	A4.1	−70	140	18.83	35.71
Duncombe Rae et al. (1996)	B1-1.1	−150	300	16.65	35.49
Duncombe Rae et al. (1996)	B2-1.1	−300	400	13.13	35.24
Duncombe Rae et al. (1996)	B2-2.1	−100	200	15.84	35.58
Duncombe Rae et al. (1996)	B2-3.1	−50	100	18.33	35.72
Duncombe Rae et al. (1996)	B2-4.1	−100	200	18.96	35.57
Duncombe Rae et al. (1996)	B3-1.1	−300	400	13.73	35.37
Arhan et al. (1999)	R1.1	−325	350	11.6	35.08
Arhan et al. (1999)	R2.1	−150	120	17.1	35.71
Arhan et al. (1999)	R3.1	−350	300	13.6	35.34
McDonagh et al. (1999)	R1.1	−325	450	13	35.2
McDonagh et al. (1999)	R2.1	−150	100	18	35.5

Note. The precision of the variables is not fixed as it depends on each article. Gordon et al. (1987), McCartney and Woodgate-Jones (1991), Duncombe Rae et al. (1992), van Ballegooyen et al. (1994), Duncombe Rae et al. (1996), Arhan et al. (1999), Garzoli et al. (1999), McDonagh et al. (1999), Schmid et al. (2003), Gladyshev et al. (2008), Arhan et al. (2011), Casanova-Masjoan et al. (2017).

Table G2
Properties of the Agulhas Ring Cores Described in the Literature

Article	Eddy core number	Depth (m)	Thickness (m)	Pt0 (°C)	PSU (psu)
Garzoli et al. (1999)	R-1.1	−100	200	16.13	35.59
Garzoli et al. (1999)	R-2.1	−510	140	12.13	35.1
Garzoli et al. (1999)	R-3.1	−270	100	15.22	35.51
Garzoli et al. (1999)	R-3.2	−350	150	14.39	35.35
Schmid et al. (2003)	JAR.1	−50	100	19	35.6
Gladyshev et al. (2008)	E3.1	−400	500	12.5	35.2
Arhan et al. (2011)	Eddy M.1	−380	550	11.8	35.15
Casanova-Masjoan et al. (2017)	ACR.1	−145	170	16.6	35.6
Casanova-Masjoan et al. (2017)	ACR.2	−400	100	13.4	35.34
Guerra et al. (2018)	Lilian.1	−200	160	16.5	35.65
Guerra et al. (2018)	Lilian.2	−480	240	12.5	35.2
This study	AR.1	−290	180	16.1	35.7
This study	AR.2	−560	100	12.9	35.3

Note. The precision of the variables is not fixed as it depends on each article. Gordon et al. (1987), McCartney and Woodgate-Jones (1991), Duncombe Rae et al. (1992), van Ballegooyen et al. (1994), Duncombe Rae et al. (1996), Arhan et al. (1999), Garzoli et al. (1999), McDonagh et al. (1999), Schmid et al. (2003), Gladyshev et al. (2008), Arhan et al. (2011), Casanova-Masjoan et al. (2017).

Appendix H: Integrated Properties of the Agulhas Rings Described in the Literature

The hydrological properties of the Agulhas Ring cores described in the litterature normalized by the properties of the RecAR are listed in the Tables H1.

Table H1
Integrated Properties of the Agulhas Rings Described in the Literature Expressed as Percentage of the Same Variables Obtained for RecAR Using the Same Parameter to Compute the Maximum Depth of Integration

Article	Eddy	Volume	HCA	SCA	Reference
McCartney and Woodgate-Jones (1991)	Eddy	46%			Trap 5×10^{-2} m s^{-1}
van Ballegooyen et al. (1994)	A3	72%	71 %	123%	T > 8°C
van Ballegooyen et al. (1994)	A4	66%	112 %	186%	T > 8°C
van Ballegooyen et al. (1994)	A5	26%	35 %	61%	T > 8°C
van Ballegooyen et al. (1994)	A6	41%	50 %	65%	T > 8°C
Duncombe Rae et al. (1996)	B1-1		8%	16%	800 m
Duncombe Rae et al. (1996)	B2-1		10%	21%	800 m
Duncombe Rae et al. (1996)	B2-2		24%	51%	800 m
Duncombe Rae et al. (1996)	B2-3		23%	50%	800 m
Duncombe Rae et al. (1996)	B2-4		18%	22%	800 m
Duncombe Rae et al. (1996)	B3-1		25%	52%	800 m
McDonagh et al. (1999)	R1	31%	23%	38%	T > 10°C
McDonagh et al. (1999)	R2	96%	26%	42%	T > 10°C
Garzoli et al. (1999)	R-1		78%	125%	1,100 m
Garzoli et al. (1999)	R-2		77%		1,100 m
Garzoli et al. (1999)	R-3		45%		1,100 m
Schmid et al. (2003)	JAR		101%	167%	1,100 m

Note. We do not compare volume for a fixed depth as this is not relevant here.

Acknowledgments
The database produced for this paper and scripts to reproduce the main figures presented in the results are available at the following: https://vesg.ipsl.upmc.fr/thredds/catalog/IPSLFS/datapapers/Laxenaire_Database_AR_Recont/catalog.html. The gridded satellite altimetry data we used in this work were produced by SSALTO/DUACS and distributed by the Copernicus Marine Environment Monitoring Service. The Argo data were collected and made freely available by the International Argo Program and the national programs that contribute to it (http://coriolis.eu.org and http://www.argo.ucsd.edu). The Argo Program is part of the Global Ocean Observing System. The GHRSST Level 4 ODYSSEA Global Foundation Sea Surface Temperature Analysis product was created by IFREMER/CERSAT with the support of the European Commission GMES Framework. This work was supported by the European Union's Horizon 2020 research and innovation program under Grant Agreement 633211 (AtlantOS) and Grant Agreement 817578 (TRIATLAS), the TOEddies CNES-TOSCA research grant, and the 11-ANR-56-004SAMOC research grant for SS and RL and the ANR-Astrid Project DYNED-Atlas (ANR-15-ASMA-0003-01) for AS and RL. The authors received several helpful suggestions for improving an earlier version of this manuscript from A. Doglioli, I. Borrione, and two anonymous reviewers, and their help is gratefully noted. We also acknowledge the mesoscale calculation server CICLAD (http://ciclad-web.ipsl.jussieu.fr) dedicated to Institut Pierre Simon Laplace modeling effort for technical and computational support.

References

Abernathey, R., & Haller, G. (2018). Transport by Lagrangian vortices in the Eastern Pacific. *Journal of Physical Oceanography*, *48*(3), 667–685. https://doi.org/10.1175/JPO-D-17-0102.1

Alfultis, M. A., & Cornillon, P. (2001). Annual and interannual changes in the North Atlantic STMW layer properties. *Journal of Physical Oceanography*, *31*(8), 2066–2086. https://doi.org/10.1175/1520-0485(2001)031<2066:AAICIT>2.0.CO;2

Amores, A., Melnichenko, O., & Maximenko, N. (2017). Coherent mesoscale eddies in the North Atlantic subtropical gyre: 3-D structure and transport with application to the salinity maximum. *Journal of Geophysical Research: Oceans*, *122*, 23–41. https://doi.org/10.1002/2016JC012256

Arhan, M., Mercier, H., & Lutjeharms, J. R. E. (1999). The disparate evolution of three Agulhas rings in the South Atlantic Ocean. *Journal of Geophysical Research Oceans*, *104* C9, 20,987-21,005. https://doi.org/10.1029/1998JC900047

Arhan, M., Speich, S., Messager, C., Dencausse, G., Fine, R., & Boye, M. (2011). Anticyclonic and cyclonic eddies of subtropical origin in the subantarctic zone south of Africa. *Journal of Geophysical Research*, *116*(C11). Retrieved from), C11004. https://doi.org/10.1029/2011jc007140

Assassi, C., Morel, Y., Vandermeirsch, F., Chaigneau, A., Pegliasco, C., Morrow, R., et al. others (2016). An index to distinguish surface-and subsurface-intensified vortices from surface observations. *Journal of Physical Oceanography*, *46*(8), 2529-2552. https://doi.org/10.1175/JPO-D-15-0122.1

Beron-Vera, F. J., Wang, Y., Olascoaga, M. J., Goni, G. J., & Haller, G. (2013). Objective detection of oceanic eddies and the Agulhas leakage. *Journal of Physical Oceanography*, *43*(7), 1426–1438. https://doi.org/10.1175/JPO-D-12-0171.1

Biastoch, A., & Böning, C. W. (2013). Anthropogenic impact on Agulhas leakage. *Geophysical Research Letters*, *40*, 1138–1143. https://doi.org/10.1002/grl.50243

Biastoch, A., Böning, C. W., & Lutjeharms, J. R. E. (2008). Agulhas leakage dynamics affects decadal variability in Atlantic overturning circulation. *Nature*, *456*(7221), 489–492. http://oceanrep.geomar.de/8189/, https://doi.org/10.1038/nature07426

Biastoch, A., Böning, C. W., Schwarzkopf, F. U., & Lutjeharms, J. (2009). Increase in Agulhas leakage due to poleward shift of Southern Hemisphere westerlies. *Nature*, *462*(7272), 495–498. https://doi.org/10.1038/nature08519

Branch, M. A., Coleman, T. F., & Li, Y. (1999). A subspace, interior, and conjugate gradient method for large-scale bound-constrained minimization problems. *SIAM Journal on Scientific Computing*, *21*(1), 1–23. https://doi.org/10.1137/S1064827595289108

Byrne, D. A., Gordon, A. L., & Haxby, W. F. (1995). Agulhas eddies: A synoptic view using Geosat ERM data. *Journal of Physical Oceanography*, *25*(5), 902917. https://doi.org/10.1175/1520-0485(1995)025<0902:AEASVU>2.0.CO;2

Cabanes, C., Thierry, V., & Lagadec, C. (2016, 8). Improvement of bias detection in Argo float conductivity sensors and its application in the North Atlantic, *Deep Sea Research Part I: Oceanographic Research Papers*, *114*, 128-136. doi: https://doi.org/10.1016/j.dsr.2016.05.007

Capuano, T. A., Speich, S., Carton, X., & Blanke, B. (2018). Mesoscale and sub- mesoscale processes in the Southeast Atlantic and their impact on the regional thermohaline structure. *Journal of Geophysical Research: Oceans*, *123*(3), 1937–1961. https://doi.org/10.1002/2017JC013396

Carton, X. (2001). Hydrodynamical modeling of oceanic vortices. *Surveys in Geophysics*, *22*(3), 179-263. https://doi.org/10.1023/A:1013779219578

Casanova-Masjoan, M., Pelegrf, J., Sangra, P., Martinez, A., Grisolia-Santos, D., Perez-Hernandez, M. D., & Hernandez-Guerra, A. (2017). Characteristics and evolution of an Agulhas ring. *Journal of Geophysical Research: Oceans*, *122*, 7049–7065. https://doi.org/10.1002/2017JC012969

Chaigneau, A., Eldin, G., & Dewitte, B. (2009). Eddy activity in the four major upwelling systems from satellite altimetry (1992-2007). *Progress in Oceanography*, *83*(1-4), 117–123. https://doi.org/10.1016/j.pocean.2009.07.012

Chaigneau, A., Gizolme, A., & Grados, C. (2008). Mesoscale eddies off Peru in altimeter records: Identification algorithms and eddy spatio-temporal patterns. *Progress in Oceanography*, *79*(2-4), 106–119. https://doi.org/10.1016/j.pocean.2008.10.013

Chaigneau, A., Marie, L. T., Gerard, E., Carmen, G., & Oscar, P. (2011). Vertical structure of mesoscale eddies in the eastern South Pacific Ocean: A composite analysis from altimetry and Argo profiling floats. *Journal of Geophysical Research: Oceans*, *116*, C11025. https://doi.org/10.1029/2011JC007134

Chelton, D. B., Schlax, M. G., & Samelson, R. M. (2011). Global observations of nonlinear mesoscale eddies. *Progress in Oceanography*, *91*(2), 167-216. https://doi.org/10.1016/j.pocean.2011.01.002

Chelton, D. B., Schlax, M. G., Samelson, R. M., & de Szoeke, R. A. (2007). Global observations of large oceanic eddies. *Geophysical Research Letters*, *34*, L15606. https://doi.org/10.1029/2007GL030812

Dash, P., Ignatov, A., Martin, M., Donlon, C., Brasnett, B., Reynolds, R. W. et al. (2012). Group for High Resolution Sea Surface Temperature (GHRSST) analysis fields inter-comparisons—Part 2: Near real time web-based level 4 SST quality monitor (L4-SQUAM). *Deep Sea Research Part II: Topical Studies in Oceanography*, *77*, 31-43. https://doi.org/10.1016/j.dsr2.2012.04.002

De Steur, L., Van Leeuwen, P., & Drijfhout, S. (2004). Tracer leakage from modeled Agulhas rings. *Journal of Physical Oceanography*, *34*(6), 1387–1399. https://doi.org/10.1175/1520-0485(2004)034<1387:TLFMAR>2.0.CO;2

Dencausse, G., Arhan, M., & Speich, S. (2010). Routes of Agulhas rings in the southeastern Cape Basin. *Deep Sea Research Part I: Oceanographic Research Papers*, *57*(11), 1406–1421. https://doi.org/10.1016/j.dsr.2010.07.008

Doglioli, A., Veneziani, M., Blanke, B., Speich, S., & Griffa, A. (2006). A Lagrangian analysis of the Indian-Atlantic interocean exchange in a regional model. *Geophysical Research Letters*, *33*, L14611. https://doi.org/10.1029/2006GL026498

Doglioli, A. M., Blanke, B., Speich, S., & Lapeyre, G. (2007). Tracking coherent structures in a regional ocean model with wavelet analysis: Application to Cape Basin eddies. *Journal of Geophysical Research*, *112*, C05043. https://doi.org/10.1029/2006JC003952

Duacs/AVISO+. (2015). *SSALTO/DUACS user handbook: (M) SLA and (M) ADT near-real time and delayed time products. CLS-DOS-NT-06-034*, *6*, 74.

Duacs/AVISO+. (2017). *Mesoscale eddy trajectory atlas product handbook*. *SALP-MU-P-EA-23126-CLS*, 17.

Duncombe Rae, C., Garzoli, S., & Gordon, A. (1996). The eddy field of the southeast Atlantic Ocean: A statistical census from the Benguela Sources and Transports Project. *Journal of Geophysical Research, Oceans*, *101*(C5), 11,949–11,964. https://doi.org/10.1029/95JC03360

Duncombe Rae, C., Shillington, F., Agenbag, J., Taunton-Clark, J., & Griindlingh, M. (1992). An Agulhas ring in the South Atlantic Ocean and its interaction with the Benguela upwelling frontal system. *Deep Sea Research Part A. Oceanographic Research Papers*, *39*(11-12), 2009–2027. https://doi.org/10.1016/0198-0149(92)90011-H

Faghmous, J. H., Frenger, I., Yao, Y., Warmka, R., Lindell, A., & Kumar, V. (2015). A daily global mesoscale ocean eddy dataset from satellite altimetry. *Scientific Data*, *2*(1), 150028. https://doi.org/10.1038/sdata.2015.28

Flierl, G. R. (1981). Particle motions in large-amplitude wave fields. *Geophysical and Astrophysical Fluid Dynamics*, *18*(1-2), 39–74. https://doi.org/10.1080/03091928108208773

Froyland, G., Horenkamp, C., Rossi, V., & Van Sebille, E. (2015). Studying an Agulhas ring's long-term pathway and decay with finite-time coherent sets. *Chaos: An Interdisciplinary Journal of Nonlinear Science*, *25*(8), 083119. https://doi.org/10.1063/1.4927830

Garzoli, S. L., Richardson, P. L., Duncombe Rae, C. M., Fratantoni, D. M., Goni, G. J., & Roubicek, A. J. (1999). Three Agulhas rings observed during the Benguela Current Experiment. *Journal of Geophysical Research*, *104*(C9), 20,971-20,985. https://doi.org/10.1029/1999JC900060

Gladyshev, S., Arhan, M., Sokov, A., & Speich, S. (2008). A hydrographic section from South Africa to the southern limit of the Antarctic Circumpolar Current at the Greenwich meridian. *Deep Sea Research Part I: Oceanographic Research Papers*, *55*(10), 1284–1303. https://doi.org/10.1016/j.dsr.2008.05.009

Goni, G., Garzoli, S., Roubicek, A., Olson, D., & Brown, O. (1997). Agulhas ring dynamics from TOPEX/POSEIDON satellite altimeter data [Article]. *Journal of Marine Research*, *55*(5), 861–883. https://doi.org/10.1357/0022240973224175

Gordon, A. L., & Haxby, W. F. (1990). Agulhas eddies invade the South Atlantic: Evidence from Geosat altimeter and shipboard conductivity-temperature-depth survey. *Journal of Geophysical Research, Oceans*, *95*(C3), 3117–3125. https://doi.org/10.1029/JC095iC03p03117

Gordon, A. L., Lutjeharms, J. R., & Griindlingh, M. L. (1987). Stratification and circulation at the Agulhas Retroflection. *Deep Sea Research Part A. Oceanographic Research Papers*, *34*(4), 565–599. https://doi.org/10.1016/0198-0149(87)90006-9

Gründlingh, M. L. (1995). Tracking eddies in the southeast Atlantic and southwest Indian oceans with TOPEX/POSEIDON. *Journal of Geophysical Research, Oceans*, *100*(C12), 24,977–24,986. https://doi.org/10.1029/95JC01985

Guerra, L. A. A., Paiva, A. M., & Chassignet, E. P. (2018). On the translation of Agulhas rings to the western South Atlantic Ocean. *Deep Sea Research Part I: Oceanographic Research Papers*, *139*, 104–113. https://doi.org/10.1016/j.dsr.2018.08.005

Hanawa, K., & Talley, L. D. (2001). Chapter 5.4 Mode waters. In G. Siedler, J. Church, & J. Gould (Eds.), *Ocean Circulation and Climate*, International Geophysics (Vol. 77, pp. 373-386). Academic Press. https://doi.org/10.1016/S0074-6142(01)80129-7

Herbette, S., Morel, Y., & Arhan, M. (2004). Subduction of a surface vortex under an outcropping front. *Journal of Physical Oceanography*, *34*(7), 1610–1627. https://doi.org/10.1175/1520-0485(2004)034<1610:SOASVU>2.0.CO;2

Ioannou, A., Stegner, A., Le Vu, B., Taupier-Letage, I., & Speich, S. (2017). Dynamical evolution of intense ierapetra eddies on a 22 year long period. *Journal of Geophysical Research: Oceans*, *122*, 9276–9298. https://doi.org/10.1002/2017JC013158

Joyce, T. M. (2012). New perspectives on eighteen-degree water formation in the North Atlantic. *Journal of Oceanography*, *68*(1), 45–52. https://doi.org/10.1007/s10872-011-0029-0

Kersalé, M., Lamont, T., Speich, S., Terre, T., Laxenaire, R., Roberts, M. J., … Ansorge, I. J. (2018, Sep). Moored observations of mesoscale features in the Cape Basin: Characteristics and local impacts on water mass distributions. *Ocean Science*, *14* (5), 923-945. https://doi.org/10.5194/os-14-923-2018

Kouketsu, S., Tomita, H., Oka, E., Hosoda, S., Kobayashi, T., & Sato, K. (2012). The role of meso-scale eddies in mixed layer deepening and mode water formation in the western North Pacific. *Journal of Oceanography*, *68*(1), 63–77. https://doi.org/10.1007/s10872-011-0049-9

Laxenaire, R., Speich, S., Blanke, B., Chaigneau, A., Pegliasco, C., & Stegner, A. (2018). Anticyclonic eddies connecting the western boundaries of Indian and Atlantic Oceans. *Journal of Geophysical Research: Oceans*, *123*(11), 7651-7677. https://doi.org/10.1029/2018JC014270

Le Vu, B., Stegner, A., & Arsouze, T. (2018). Angular Momentum Eddy Detection and tracking Algorithm (AMEDA) and its application to coastal eddy formation. *Journal of Atmospheric and Oceanic Technology*, *35*(4), 739–762. https://doi.org/10.1175/JTECH-D-17-0010.1

Lebedev, K. V., Yoshinari, H., Maximenko, N. A., & Hacker, P. W. (2007). Velocity data assessed from trajectories of Argo floats at parking level and at the sea surface . *IPRC Technical Note*, *4*(2), 1–16.

Lehahn, Y., d'Ovidio, F., Levy, M., Amitai, Y., & Heifetz, E. (2011). Long range transport of a quasi isolated chlorophyll patch by an Agulhas ring. *Geophysical Research Letters*, *38*, n/a. https://doi.org/10.1029/2011GL048588

Lumpkin, R. (2016). Global characteristics of coherent vortices from surface drifter trajectories. *Journal of Geophysical Research: Oceans*, *121*, 1306–1321. https://doi.org/10.1002/2015JC011435

Martin, M., Dash, P., Ignatov, A., Banzon, V., Beggs, H., Brasnett, B. et al. (2012). Group for High Resolution Sea Surface Temperature (GHRSST) analysis fields inter-comparisons. Part 1: A GHRSST multi-product ensemble (GMPE). *Deep Sea Research Part II: Topical Studies in Oceanography*, *77*, 21-30. https://doi.org/10.1016/j.dsr2.2012.04.013

McCartney, M. (1977). *Subantarctic mode water, a voyage of discovery, George Deacon: 70th Anniversary Volume M. Angel, 103-119*. New York: Pergamon.

McCartney, M. S. (1982). The subtropical recirculation of mode waters. *Journal of Marine Research*, *40*(427.4), 64.

McCartney, M. S., & Woodgate-Jones, M. (1991). A deep-reaching anticyclonic eddy in the subtropical gyre of the eastern South Atlantic. *Deep Sea Research Part A. Oceanographic Research Papers*, *38*, S411–S443. https://doi.org/10.1016/S0198-0149(12)80019-7

McDonagh, E. L., Heywood, K. J., & Meredith, M. P. (1999). On the structure, paths, and fluxes associated with Agulhas rings. *Journal of Geophysical Research, Oceans*, *104*(C9), 21,007–21,020. https://doi.org/10.1029/1998JC900131

McDougall, T. J., & Barker, P. M. (2011). *Getting started with TEOS-10 and the Gibbs Seawater (GSW) oceanographic toolbox*. SCOR/IAPSO WG (Vol. 127, pp. 128). ISBN 978-0-646-55621-5.

McWilliams, J. C. (1985). Submesoscale, coherent vortices in the ocean. *Reviews of Geophysics*, *23*(2), 165–182. https://doi.org/10.1029/RG023i002p00165

Mkhinini, N., Coimbra, A. L. S., Stegner, A., Arsouze, T., Taupier-Letage, I., & Beranger, K. (2014). Long-lived mesoscale eddies in the eastern Mediterranean Sea: Analysis of 20 years of AVISO geostrophic velocities. *Journal of Geophysical ResearchL: Oceans*, *119*(12), 8603-8626. https://doi.org/10.1002/2014JC010176

Morrow, R., & Le Traon, P.-Y. (2012). Recent advances in observing mesoscale ocean dynamics with satellite altimetry. *Advances in Space Research*, *50*(8), 1062–1076. https://doi.org/10.1016/j.asr.2011.09.033

Nencioli, F., Dall'Olmo, G., & Quartly, G. D. (2018). Agulhas ring transport efficiency from combined satellite altimetry and Argo profiles. *Journal of Geophysical Research: Oceans*, *123*(8), 5874–5888. https://doi.org/10.1029/2018JC013909

Nencioli, F., Dong, C., Dickey, T., Washburn, L., & McWilliams, J. C. (2010). A vector geometry-based eddy detection algorithm and its application to a high-resolution numerical model product and high-frequency radar surface velocities in the Southern California Bight. *Journal of Atmospheric and Oceanic Technology*, *27*(3), 564-579. https://doi.org/10.1175/2009JTECHO725.1

Olson, D. B., & Evans, R. H. (1986). Rings of the Agulhas current. *Deep Sea Research Part A. Oceanographic Research Papers*, *33*(1), 27–42. https://doi.org/10.1016/0198-0149(86)90106-8

Owens, W. B., & Wong, A. P. (2009). An improved calibration method for the drift of the conductivity sensor on autonomous CTD profiling floats by 0-S climatology. *Deep Sea Research Part I: Oceanographic Research Papers*, *56*(3), 450–457. https://doi.org/10.1016/j.dsr.2008.09.008

Pegliasco, C., Chaigneau, A., & Morrow, R. (2015). Main eddy vertical structures observed in the four major Eastern Boundary Upwelling Systems. *Journal of Geophysical Research: Oceans*, *120*, 6008–6033. https://doi.org/10.1002/2015JC010950

Provost, C., Escoffier, C., Maamaatuaiahutapu, K., Kartavtseff, A., & Garcon, V. (1999). Subtropical mode waters in the South Atlantic Ocean. *Journal of Geophysical Research, Oceans*, *104*(C9), 21,033–21,049. https://doi.org/10.1029/1999JC900049

Pujol, M.-I., Faugere, Y., Taburet, G., Dupuy, S., Pelloquin, C., Ablain, M., & Pi- cot, N. (2016). DUACS DT2014: The new multi-mission altimeter data set reprocessed over 20 years. *Ocean Science*, *12*(5), 1067–1090. https://doi.org/10.5194/os-12-1067-2016

Rusciano, E., Speich, S., & Ollitrault, M. (2012). Interocean exchanges and the spreading of Antarctic Intermediate Water south of Africa. *Journal of Geophysical Research, Oceans*, *117*(C10), n/a. https://doi.org/10.1029/2012JC008266

Sato, O., & Polito, P. (2014). Observation of South Atlantic subtropical mode waters with Argo profiling float data. *Journal of Geophysical Research: Oceans*, *119*, 2860–2881. https://doi.org/10.1002/2013JC009438

Schmid, C., Boebel, O., Zenk, W., Lutjeharms, J., Garzoli, S., Richardson, P., & Barron, C. (2003). Early evolution of an Agulhas Ring. *Deep Sea Research Part II: Topical Studies in Oceanography*, *50*(1), 141–166. https://doi.org/10.1016/S0967-0645(02)00382-X

Schouten, M. W., de Ruijter, W. P. M., van Leeuwen, P. J., & Lutjeharms, J. R. E. (2000). Translation, decay and splitting of Agulhas rings in the southeastern Atlantic Ocean. *Journal of Geophysical Research*, *105*(C9), 21,913–21,925. https://doi.org/10.1029/1999JC000046

Schütte, F., Brandt, P., & Karstensen, J. (2016). Occurrence and characteristics of mesoscale eddies in the tropical northeast Atlantic Ocean. *Ocean Science*, *12*(3), 663–685. https://doi.org/10.5194/os-12-663-2016

Smith, W., & Sandwell, D. (1997). Global sea floor topography from satellite altimetry and ship depth soundings. *Science*, *277*(5334), 1956–1962. https://doi.org/10.1126/science.277.5334.1956

de Souza, A. G. Q., Kerr, R., & de Azevedo, J. L. L. (2018). On the influence of subtropical mode water on the South Atlantic Ocean. *Journal of Marine Systems*, *185*, 13–24. https://doi.org/10.1016/j.jmarsys.2018.04.006

Souza, J., Chapron, B., & Autret, E. (2014). The surface thermal signature and air- sea coupling over the Agulhas rings propagating in the South Atlantic Ocean interior. *Ocean Science*, *10*(4), 633–644. https://doi.org/10.5194/os-10-633-2014

Souza, J. M. A. C., de Boyer Montegut, C., Cabanes, C., & Klein, P. (2011). Estimation of the Agulhas ring impacts on meridional heat fluxes and transport using ARGO floats and satellite data. *Geophysical Research Letters*, *38*, L21602. https://doi.org/10.1029/2011GL049359

Stammer, D. (1997). Global characteristics of ocean variability estimated from regional TOPEX/POSEIDON altimeter measurements. *Journal of Physical Oceanography*, *27*(8), 1743–1769. https://doi.org/10.1175/1520-0485(1997)027<1743:GCOOVE>2.0.CO;2

van Ballegooyen, R. C., Grnndlingh, M. L., & Lutjeharms, J. R. E. (1994). Eddy fluxes of heat and salt from the southwest Indian Ocean into the southeast Atlantic Ocean: A case study. *Journal of Geophysical Research*, *99*(C7), 14,053–14,070. https://doi.org/10.1029/94JC00383, https://doi.org/10.1029/94JC00383

van Sebille, E., & van Leeuwen, P. J. (2007). Fast northward energy transfer in the Atlantic due to Agulhas rings. *Journal of Physical Oceanography*, *37*(9), 23052315. https://doi.org/10.1175/JPO3108.1

Wang, Y., Beron-Vera, F., & Olascoaga, M. (2016). The life cycle of a coherent Lagrangian Agulhas ring. *Journal of Geophysical Research: Oceans*, *121*, 3944–3954. https://doi.org/10.1002/2015JC011620

Wang, Y., Olascoaga, M., & Beron-Vera, F. (2015). Coherent water transport across the South Atlantic. *Geophysical Research Letters*, *42*, 4072–4079. https://doi.org/10.1002/2015GL064089

Weijer, W., De Ruijter, W. P., & Dijkstra, H. A. (2001). Stability of the Atlantic overturning circulation: Competition between Bering Strait freshwater flux and Agulhas heat and salt sources. *Journal of Physical Oceanography*, *31*(8), 2385–2402. https://doi.org/10.1175/1520-0485(2001)031<2385:SOTAOC>2.0.CO;2

Weijer, W., de Ruijter, W. P., Dijkstra, H. A., & Van Leeuwen, P. J. (1999). Impact of interbasin exchange on the Atlantic overturning circulation. *Journal of Physical Oceanography*, *29*(9), 2266–2284. https://doi.org/10.1175/1520-0485(1999)029<2266:IOIEOT>2.0.CO;2

Weijer, W., De Ruijter, W. P., Sterl, A., & Drijfhout, S. S. (2002). Response of the Atlantic overturning circulation to South Atlantic sources of buoyancy. *Global and Planetary Change*, *34*(3-4), 293–311. https://doi.org/10.1016/S0921-8181(02)00121-2

Williams, R. (2001). Ocean subduction. In J. H. Steele (Ed.), *Encyclopedia of ocean sciences* (pp. 1982-1993). Oxford: Academic Press. https://doi.org/10.1006/rwos.2001.0109

Wunsch, C. (1999). Where do ocean eddy heat fluxes matter?. *Journal of Geophysical Research Oceans (1978-2012)*, *104*(C6), 13,235–13,249. https://doi.org/10.1029/1999JC900062

Zeitlin, V. (2018). *Geophysical fluid dynamics: Understanding (almost) everything with rotating shallow water models*. Oxford: Oxford University Press. https://doi.org/10.1093/oso/9780198804338.001.0001